Helicopter-Borne Sensors Monitoring Pack Ice Properties of Mackenzie Delta April 2010 Sea Ice Survey

S.J. Prinsenberg, I.K. Peterson, J.S. Holladay and L. Lalumiere

Ocean Sciences Division
Maritimes Region
Fisheries and Oceans Canada

Bedford Institute of Oceanography
P.O. Box 1006
Dartmouth, Nova Scotia
Canada B2Y 4A2

2010

Canadian Technical Report of Hydrography and Ocean Sciences 267

Fisheries and Oceans Canada | Pêches et Océans Canada

Canada

Canadian Technical Report of Hydrography and Ocean Sciences

Technical reports contain scientific and technical information of a type that represents a contribution to existing knowledge but which is not normally found in the primary literature. The subject matter is generally related to programs and interests of the Oceans and Science sectors of Fisheries and Oceans Canada.

Technical reports may be cited as full publications. The correct citation appears above the abstract of each report. Each report is abstracted in the data base *Aquatic Sciences and Fisheries Abstracts.*

Technical reports are produced regionally but are numbered nationally. Requests for individual reports will be filled by the issuing establishment listed on the front cover and title page.

Regional and headquarters establishments of Ocean Science and Surveys ceased publication of their various report series as of December 1981. A complete listing of these publications and the last number issued under each title are published in the *Canadian Journal of Fisheries and Aquatic Sciences*, Volume 38: Index to Publications 1981. The current series began with Report Number 1 in January 1982.

Rapport technique canadien sur l'hydrographie et les sciences océaniques

Les rapports techniques contiennent des renseignements scientifiques et techniques qui constituent une contribution aux connaissances actuelles mais que l'on ne trouve pas normalement dans les revues scientifiques. Le sujet est généralement rattaché aux programmes et intérêts des secteurs des Océans et des Sciences de Pêches et Océans Canada.

Les rapports techniques peuvent être cités comme des publications à part entière. Le titre exact figure au-dessus du résumé de chaque rapport. Les rapports techniques sont résumés dans la base de données *Résumés des sciences aquatiques et halieutiques.*

Les rapports techniques sont produits à l'échelon régional, mais numérotés à l'échelon national. Les demandes de rapports seront satisfaites par l'établissement auteur dont le nom figure sur la couverture et la page de titre.

Les établissements de l'ancien secteur des Sciences et Levés océaniques dans les régions et à l'administration centrale ont cessé de publier leurs diverses séries de rapports en décembre 1981. Vous trouverez dans l'index des publications du volume 38 du *Journal canadien des sciences halieutiques et aquatiques*, la liste de ces publications ainsi que le dernier numéro paru dans chaque catégorie. La nouvelle série a commencé avec la publication du rapport numéro 1 en janvier 1982.

Canadian Technical Report of Hydrography and Ocean Sciences 267

2010

Helicopter-borne sensors monitoring pack ice properties of Mackenzie Delta April 2010 Sea Ice Survey

by

Simon J. Prinsenberg, Ingrid K. Peterson, J. Scott Holladay[1] and Louis Lalumiere[2]

Ocean Sciences Division
Maritimes Region
Fisheries and Oceans Canada
Bedford Institute of Oceanography
P.O. Box 1006
Dartmouth, N.S., B2Y 4A2

[1] Geosensors Inc., 66 Mann Ave.,
Toronto, Ontario, M4S 2Y3

[2] Sensors by Design Ltd., 100 Peevers Crescent,
Newmarket, Ontario, L3Y 7T1

© Her Majesty the Queen in Right of Canada 2010
Cat. No. FS 97-18/267E ISSN 0711-6764

Correct citation for this publication:
Prinsenberg, S.J., I.K. Peterson, J.S. Holladay and L. Lalumiere, 2010. Helicopter-borne sensors monitoring the pack ice properties of Mackenzie Delta April 2010 Sea Ice Survey. Can Tech. Rep. Hydrogr. Ocean Sci. 267: viii+62pp.

Table of Contents ..... Page

List of Figures iv
List of Tables vii
Abstract/Résumé viii

Introduction 1
Instrumentation 2
Electromagnetic-Laser Sensor 2
Ground Penetrating Radar 4
Video-Laser System 4
GPS Sensors 5

Survey Description 5

Data Samples 10
EM Data 11
GPR Data 14
Video Data 18
On-Ice Data 23

Combining EM-GPR-Video-Photographs 26
Small Lead 26
Other figures for FEM1003 (April 1) 28
Bottom-Fast Ice (BFI) 28
Inshore Gravel Bar 32
Bare Ice Areas 35
Ridges and Leads 38

Conclusion 44

Acknowledgement 44

References 44

Appendix 1: Station List 46
Appendix 2: Field Notes 47
Appendix 3: GPR post processing 53

List of Figures

Fig. 1 Mackenzie Delta flight lines and station numbers for April 2010 ice survey. Bottom contour lines show the depths in meters. Inuvik was the overnight base for the survey with fuel depots at Swimming Point and Tuktoyaktuk. Stations' lat/long values are listed in Appendix 1.
Fig. 2 Canadian Helicopter 206L at the Inuvik airport showing the fix-mounted sensor equipment. The EM sensor is located in the front section and the GPR and video-laser are located in the middle section of the "cigar" shaped mount.
Fig. 3 Sensors and Software Noggin 1000-NIC GPR System (left) and protruding from middle section of the mounting tube along with laser/video camera (right).
Fig. 4 GPR data line sections flown on April 1 overlain on a RADARSAT-2 SAR image of April 3 (© RADARSAT-2 Data and Products © MacDonald, Dettwiler and Associates Ltd. (2010)- All Rights Reserved).
Fig. 5 GPR data line sections flown on April 5 overlain on a RADARSAT-2 SAR image of April 3 (© RADARSAT-2 Data and Products © MacDonald, Dettwiler and Associates Ltd. (2010)- All Rights Reserved).
Fig. 6 GPR data line sections flown on April 8 overlain on a RADARSAT-2 SAR image of April 3 (© RADARSAT-2 Data and Products © MacDonald, Dettwiler and Associates Ltd. (2010)- All Rights Reserved).
Fig. 7 GPR data line sections flown on April 9 overlain on a RADARSAT-2 SAR image of April 3 (© RADARSAT-2 Data and Products © MacDonald, Dettwiler and Associates Ltd. (2010)- All Rights Reserved).
Fig. 8 Laser time series profile of the survey line between Stns. 5, 2 and 3.
Fig. 9 Ice thickness and ice roughness "Quick-look" profile plot for the line section between Stns. 5 and 2 collected on the afternoon of April 1.
Fig. 10 Ice thickness and ice roughness "Quick-look" profile plot for the line section between Stns. 2 and 3 collected on the afternoon of April 1.
Fig. 11 Ice thickness plot of the sub-section covering the mobile ice near Stn. 17 where the IOS mooring is located.
Fig. 12 Quick-look GPR time series plot of line sub-section F656 of April 1. It covers about 4km along the horizontal axis and about 6m along the vertical axis.
Fig. 13 High-resolution display of GPR data for a F656 sub-section collected in the afternoon of April 1. Snow depths up to 1m are plotted along the bottom panel but only represent true snow depths when the third bottom echo is weak or absent.
Fig. 14 First part of the GPR section F660 passing over a major rubble area (#1000), where very deep snow accumulated in the rough surface ice topography. The vertical scale in the top panel provides the height with respect to the propagation of radar waves in air, and thus overestimates the snow and ice thickness.
Fig. 15 Offshore part of the GPR section F660 passing over another rubble field beyond which the GPR starts losing the bottom ice echo due to increased brine volume.
Fig. 16 Start of GPR section F661 showing the faint bottom ice echo and then the start of the rough ice topography (#1700). Very little snow is present over the flat ice.
Fig. 17 GPR section from F655 (~5km) showing the GPR data and annotated colour lines denoting the top of the snow layer (green line), the bottom of the snow layer (red line) and the bottom of the ice cover (turquoise line). The resulting snow depth and ice

thickness profiles are shown in the lower panels. The vertical scale in the top panel provides the height with respect to the propagation of radar waves in air, and thus overestimates the snow and ice thickness.
Fig. 18 Video image of the small lead passed over on April 1 from Stn. 17 to Stn. 16, frame #6518. The middle, right of the image is unclear due some water on the outside lens cover.
Fig. 19 "Quick-look" mosaic of 37 video frames around the start of the 10 minute file folder showing the frames collected between 12:50 and 13:00 MDT when the lead shown in Fig. 17 was seen.
Fig. 20 Mosaic line pattern flown over Minuk rubble field on April 9.
Fig. 21 Mosaic video frames collected over the Tarsiut rubble field on April 9.
Fig. 22 Location map of on-ice station visited on April 8, 2010. (© RADARSAT-2 Data and Products © MacDonald, Dettwiler and Associates Ltd. (2010) - All Rights Reserved).
Fig. 23 Salinity-temperature profile of Stn. 46 from April 8, 2010.
Fig. 24 Salinity-temperature profile of Stn. 47 from April 8, 2010.
Fig. 25 Photo of small ridge/lead taken at 100m altitude between stations 16 and 17 on April 1.
Fig. 26 The fifth of six EM sub-sections along the flight line between Stns. 15 and 17.
Fig. 27 Profile extracted from FEM10003; narrow lead shown as a decrease in ice thickness in the middle of the plot. Profile runs south to north and vertical gridlines are 10 seconds or approximately 300m apart.
Fig. 28 GPR plot section for F560 where the small lead occurs, and is shown by two laser peaks at sample #2150.
Fig. 29 FEM10003 Pic profile plot of sub-section 5 where the small lead was present and shown by the expanded plot in Fig. 27. Apparent water conductivity continues to rise, mainly at thick ridges that cause ponding of freshwater under ice.
Fig. 30 FEM10003 Pic profile plot of the offshore sub-section 6. It covers the offshore mobile ice area where Stn. 27 (IOS mooring) was beneath the rough rubble field and shown also in Fig. 11. Note multiple increases in apparent water conductivity, with the northernmost refrozen lead section just below 2 S/m.
Fig. 31 "Quick-look" ice thickness profile plot for total FEM10006 line of April 1.
Fig. 32 EM upper layer thickness and other variables for FEM10006 inshore sub-section on April 1.
Fig. 33 Quick-look GPR plot a GPR section F654.
Fig. 34 GPR images for south and north edges of first major BFI feature in Fig. 32.
Fig. 35 EM data plot aligned with the two GPR plots of Fig. 34.
Fig. 36 GPR plots of the edges of the second major BFI feature shown in Fig. 33.
Fig. 37 EM data plot aligned with the two GPR plots of Fig. 36.
Fig. 38 Gravel bar seen inshore along the flight line between Stns. 5 and 2.
Fig. 39 First section of the EM data along the flight line between Stns. 5 and 2 of April 1.
Fig. 40 GPR section plot covering ~1500m showing the gravel bar location.
Fig. 41 Detailed EM parameter plot covering the gravel bar region and covering the same spatial area as shown in Fig. 39. The ice-bonded feature and gravel bar between fids 42140 and 42150 in plot above correspond to GPR scan range 5500 to 6500.

Fig. 42 Video frame 13240 showing the gravel bed collected on April1, 16:35. The video data were collected on the way back (south) so the top of the image is the inshore end.
Fig. 43 Photo taken along video flight from line 2 to 5 (April 1) looking south.
Fig. 44 Mosaic of the bare ice feature made from four overlapping frames of April 1 at 16:22, frame #12587.
Fig. 45 Detailed EM parameter plot of second sub-section of FEM100009, line from Stn. 5 to Stns. 2 and 3.
Fig. 46 GPR sub-section plots of file # 660 representing the second GPR section along the line between stations 5 and 2 on April 1.
Fig. 47 EM quick plot showing the EM data along the same sub-section as for the GPR plot above, where the bare ice occurred south of the rough area that started at sample number $1.08x10^4$ and shown in the right panel of Fig. 46. At this place the EM inferred upper layer thickness started to follow the bottom of the freshwater plume layer rather than the ocean bottom, and the GPR ice-bottom echo faded due to increased brine volume of the ice cover.
Fig. 48 Rough ice along the April 1 flight path and identified as the 3th EM sub-section FEM10009.
Fig. 49 Quick-look upper-layer thickness profile data plot of 3th sub-section of FEM1009, April 1.
Fig. 50 Sub-segment 3 for FEM10009. Location of ridge shown in Fig. 48 is indicated in figure.
Fig. 51 Sub-section of the turning loop just past Stn. 2 showing the small lead with low ice thickness, just before a ridge feature.
Fig. 52 Small lead northwest of Stn. 2, 16:13, April 1, frame F034-11658. With an video frame width of ~100m, the lead is about ~15m wide. The top is toward the northwest.
Fig. 53 Mosaic of small second lead (Fig. 52) and ridge observed along the start of the line between Stn. 2 and Stn. 5, April 1, 16:13 Video file F034. . The left is towards the northwest.
Fig. 54 Quick-look plot of upper-layer thickness for sub-section 5 of FEM10009 on April 1. The location where the profile thickness data was collected is shown by the green line.
Fig. 55 Sub-section 5 of FEM10009. The water conductivity reached its maximum near the start of this segment and declined toward the eastern end. Note the 0.3m refrozen lead near right side, with corresponding dip (upward-pointing arrow) in normalized laser intensity.
Fig. 56 Left photo is the thin lead with 0.3m thick ice and low laser reflectivity; the right photo is of the older, deformed lead with 0.8m thick ice that shows higher laser reflectivity.
Fig. 57 Video frame #10527-F033 of April 1, 16:02 MDT showing edge of lead with ice thickness of 30cm,.
Fig. 58 Video frame #10568-F033 of April1, 16:02 MDT showing edge of lead with an ice thickness of 80cm.
Fig. 59 Mosaic of lead with ice thickness of 30cm along line from St. 3 to Stn. 2 April 1, 16:02 MDT.
Fig. 60 Mosaic of lead with ice thickness of 80cm along line from Stn. 3 to Stn. 2 on April 1, 16:02 MDT.

List of Tables

Table 1: Mackenzie Delta 2010 GPR and EM files.
Table 2: Mackenzie Delta 2010 Video and EM-Laser files.
Table 3: Mackenzie Delta 2010 on-ice station data (April 8, 2010).

Abstract

Prinsenberg, S.J., I.K. Peterson, J.S. Holladay and L. Lalumiere, 2010. Helicopter-borne sensors monitoring the pack ice properties of Mackenzie Delta: April 2010 Sea Ice Survey. Can Tech. Rep. Hydrogr. Ocean Sci. 267: viii+62pp.

This report presents examples of a unique data set that was collected with helicopter-borne sensors during April 2010 over the Mackenzie Delta land-fast and mobile ice cover areas. Helicopter logistic support was provided by the Canadian Helicopter Company in Inuvik, NWT which was used as a base for the entire survey. For the first time a Ground-Penetrating-Radar provided snow depths and ice thicknesses of low salinity ice and complemented the Electromagnetic-Laser and Video-Laser data sets to explain the ice and snow properties found in the Mackenzie Delta. In spite of numerous weather delays, the survey completed most of its planned pack ice survey lines and provides a large spatial distribution of data to derive ice and snow statistics and to validate ice signatures seen in RADARSAT-2 and TerraSAR-X SAR imagery. All data, plots, photographs and reports will be available through the DFO Maritimes Region's "SeaIce" Website: http://www.mar.dfo-mpo.gc.ca/science/ocean/seaice/public.html and its data link on the DFO Maritimes Region's FTP site: ftp://starfish.mar.dfo-mpo.gc.ca/pub/ocean/seaice/.

Résumé

Prinsenberg, S.J., I.K. Peterson, J.S. Holladay and L. Lalumiere, 2010. Helicopter-borne sensors monitoring the pack ice properties of Mackenzie Delta: April 2010 Sea Ice Survey. Can Tech. Rep. Hydrogr. Ocean Sci. 267: viii+62pp.

Ce rapport présente des exemples tirés d'un ensemble unique de données recueillies par capteurs héliportés lors d'un vol au-dessus des régions recouvertes de glaces fixes et mobiles du Delta du Mackenzie, en avril 2010. La Canadian Helicopter Company d'Inuvik, dans les Territoires du Nord-Ouest, a fourni les services d'hélicoptère et a servi de centre logistique pour toute la durée de l'étude. Pour la première fois, un géoradar a indiqué la profondeur de la neige et l'épaisseur de la glace de faible salinité, et fourni des données complémentaires à celles recueillies par laser électromagnétique et vidéo-laser; ces données permettront d'expliquer les propriétés de la neige et de la glace observées dans le Delta du Mackenzie. Malgré les nombreux retards causés par les conditions météorologiques, la majorité des lignes de levé de la banquise prévues dans le relevé ont été terminées. L'étude a fourni une large distribution spatiale des données permettant d'établir des statistiques sur la glace et la neige et de valider les signatures de la glace observées par des satellites à imagerie SAR, le RADARSAT-2 et le TerraSAR-X. L'ensemble des données, graphiques, photographies et rapports seront disponibles dans la section portant sur l'étude des glaces de mer du site Web du ministère des Pêches et des Océans – Région des Maritimes (http://www.mar.dfo-mpo.gc.ca/science/ocean/seaice/public.html). La liaison de données est disponible sur le site FTP du MPO – Région des Maritimes (ftp://starfish.mar.dfo-mpo.gc.ca/pub/ocean/seaice/).

Introduction

Changes in the Arctic Ocean weather and ice regime have received much attention in the scientific literature as well as the popular press. It is now well accepted that changes are widespread, in some cases dramatic, and that overall warming of the full Arctic system has occurred in the first decade of the twenty-first century (Richter Menge et al., 2008). Fissel et al. (2009) described the changes and trends observed over the past several years for meteorological and sea-ice conditions on the continental shelf and slope regions of the Canadian Beaufort Sea. They found that the air temperatures have clearly risen by 2-4 °C while trends in the monthly surface winds are relatively small in relation to the large degree of inter-annual variability. Land-fast ice durations and thickness are reduced in association with increasing air temperatures and snow cover. A trend towards reduced sea ice concentrations is evident for most locations and times of the year, the trend is small at -2 to -3 % per decade. Larger trends (- 6 to -11 %) of reduced ice cover were computed in the late summer ice concentrations in the Alaskan Beaufort Sea, the Canada Basin and the Seasonal Sea Ice Zone beyond the continental shelf edge. This is similar to the trend towards reduced sea ice extent in the entire Arctic Ocean of -11% in late summer. Changes including long-term trends in the atmospheric and ice cover properties are important to the development of oil and gas exploration, marine navigation, marine ecosystem and northerner's way of live within the northern ice and weather environments.

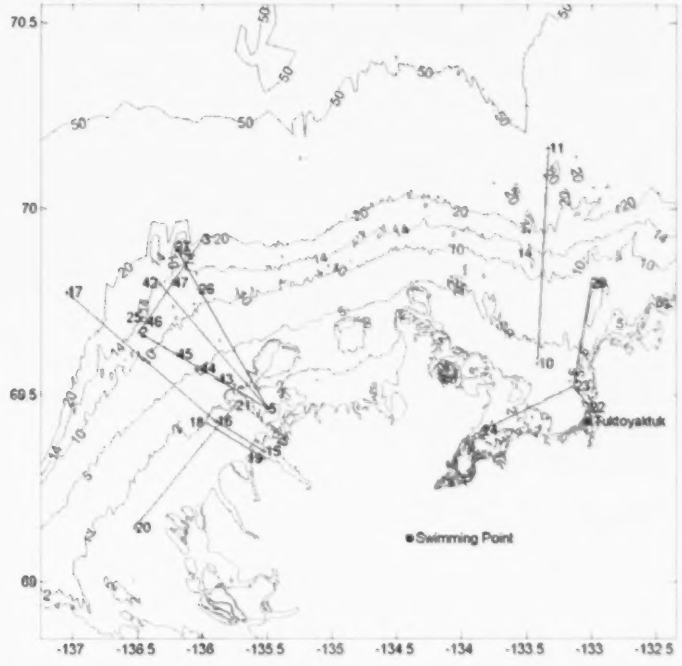

Fig. 1 Mackenzie Delta flight lines and station numbers for April 2010 ice survey. Bottom contour lines show the depths in meters. Inuvik was the overnight base for the survey with fuel depots at Swimming Point and Tuktoyaktuk. Stations' lat/long values are listed in Appendix 1.

Since the early 1990s, ice property data have been collected with helicopter-borne sensors by personnel of the Bedford Institute of Oceanography of Dartmouth, N.S. in partnership with Canadian companies (Peterson et al., 2003). The helicopter-borne electromagnetic (HEM) system (called "Ice Pic") measures ice-plus-snow thickness and ice-surface roughness. The Ground Penetrating Radar (GPR) sensor measures snow-depth over the sea ice cover and as well as ice thickness of low ice salinity (Lalumiere and Prinsenberg, 2009). The Video-GPS Sensor system collects video images to make mosaics from overlapping video frames. The sensors' observations provide information on level and deformed ice fractions, snow depths, lead and ridge and floe size distributions, all used to validate operational algorithms for inferring sea ice properties from satellite SAR imagery in ice-chart production. The data are also used to narrow the uncertainty of ice thickness and snow depth distributions required as inputs to international offshore operational codes; and are further used in research of ice-ocean-atmosphere interaction processes, validation of ice-ocean model simulations and studies of marine ecosystems.

In this report a unique data set is presented that was collected during April 2010 over the Mackenzie Delta's land-fast and mobile ice cover. Helicopter logistic support was provided by the Canadian Helicopter Company stationed in Inuvik which was used as a base for the entire survey. Weather permitting, daily survey trips were accomplished by flying to-from the pack ice from Inuvik and using fuel stations at Swimming Point and Tuktoyaktuk (Fig. 1). In spite of the weather delays, the survey completed most of its planned survey lines over to pack ice and will provide a large spatial data distribution to derive ice and snow statistics from and to validate ice signatures seen in SAR imagery. The survey included flight lines over bottom-fast ice in the near-shore area, as well as fine-scale grid flight lines over the rubble fields at the Minuk I-53 artificial island site (Stn. 25) and the Tarsiut N-44 Caisson site (Stn. 27). All results, observations and reports will be available on the DFO's Maritimes Website: http://www.mar.dfo-mpo.gc.ca/science/ocean/seaice/public.html and through its data link on the DFO Maritimes FTP site: ftp://starfish.mar.dfo-mpo.gc.ca/pub/ocean/seaice/.

Instrumentation

Electromagnetic-Laser Sensor

During the 10-day field survey, ice thickness and ice surface roughness were measured with a helicopter-borne electromagnetic (HEM) system, called the "Ice Pic", built by Geosensors Inc. of Toronto, Canada. It consists of a cigar-shaped sensor package mounted beneath and in front of the Bell 206L helicopter (Fig. 2). The helicopter used during the survey was supplied by the Canadian Helicopter Company in Inuvik, NWT. The sensor package consists of an electromagnetic (EM) sensor with transmitter and receiver coils (transmitter frequencies of 1.7, 5.0, 11.7 and 35.1 kHz) and a laser altimeter. The laser altimeter data provides ice-surface roughness profiles, laser intensity

profiles, and the height of the EM sensor above the pack ice. The laser is an ADM 3-Alpha Geophysical unit and has a listed accuracy of 1.5cm.

The EM sensor measures the distance to the ocean surface water as it is the nearest conductor, and the laser measures the distance to the pack ice surface. Together they provide the snow-plus-ice thickness. The sampling rate for the ice thickness and roughness data is 10Hz, corresponding to a spatial sampling interval of about 3-4m for the normal helicopter survey speed of 80mph. The ice thickness and ice conductivity are estimated with a 2-layer inversion model representing ice and seawater layers. The calculations are done in real-time on a computer strapped in the back seat of the helicopter and results displayed approximately 1sec later on a hand-held monitor used by the operator. Since four frequencies are available, three unknown parameters can be estimated by the post-processing inversion model. Thus the conductivity of the sea water layer can also be estimated, in addition to the ice thickness and ice conductivity.

Fig. 2 Canadian Helicopter 206L at the Inuvik airport showing the fix-mounted sensor equipment. The EM sensor is located in the front section and the GPR and Video-Laser are located in the middle section of the "cigar" shaped mount.

The footprint size of the EM sensor depends on the height of the EM sensor above the seawater (Kovacs et al., 1995) and is 16-20m for the "Ice Pic" flying at 4m over 2m thick ice. Several studies have validated the EM ice thicknesses collected by both the "Ice Pic" and "Ice Probe", a towed HEM system, by comparing EM ice thicknesses successfully with ice and snow thicknesses measured via holes drilled through the ice (Peterson et al., 2003 and Prinsenberg et al., 2008). For flat homogeneous ice over sea

water such as refrozen leads, no difference can seen between auger observations and EM helicopter data, as the differences are usually smaller than the variability in each data set. Over rough deformed ice, one has to average the auger holes to match the footprint size of the EM sensor, and once this is done the data sets again match normally within ±5cm (Peterson et al., 2003 and Prinsenberg et al., 2008).

Ground Penetrating Radar

Ground Penetrating Radars (GPRs) have the capability to measure snow thickness or fresh water ice thickness (Lalumiere and Prinsenberg, 2009). Past developments have produced one-dimensional processing algorithms for snow thickness measurement over sea ice or fresh water ice thickness. The algorithm is used to display the data in real-time on a logging laptop operated in the helicopter to ensure data are being collected.

The GPR system used is a Noggin-NIC 1000 from Sensors and Software Inc. of Mississauga, Ontario. A photograph of a Noggin-NIC 1000 is shown in Fig. 3 (Left panel). The Noggin 1000-NIC is 30cm long by 15cm wide and 12cm high. The GPR system was mounted in the middle section of the 206L mount, with its bottom plate protruding outside the tube exterior (Fig. 3, Right panel). The Noggin-NIC 1000 is a unique GPR system as it permits operation and control by a computer with no user interaction. This permits the integration of this GPR as an additional sensor for the Video-Sensor System. The Noggin-NIC 1000 is a very high resolution GPR system, with center frequency of 1000 MHz and a waveform sampling interval of 0.1 nanoseconds. The Noggin-NIC was configured to collect 500 points per scan with 4 internal stacks. This results in a scan rate of approximately 30 scans per second. When flying at 80 knots, the ground sample spacing is approximately one sample per 1.5m. This fine spacing permits the GPR to collect snow features at the same fine scale as the Laser does for surface pack ice roughness.

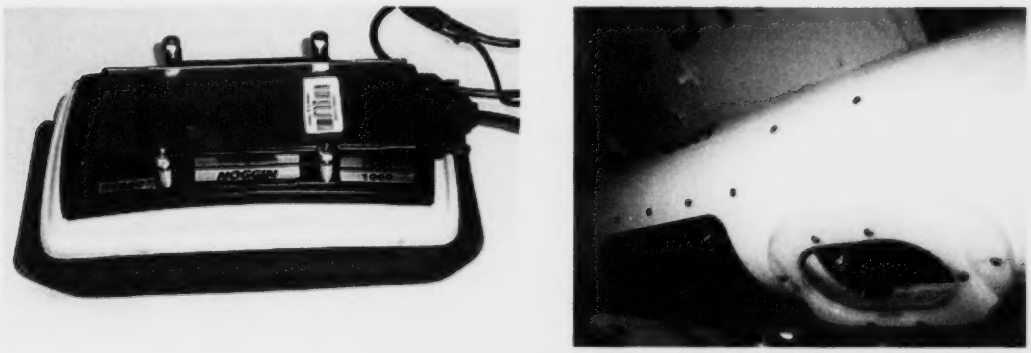

Fig. 3 Sensors and Software Noggin 1000-NIC GPR System (left) and protruding from middle section of the mounting tube along with laser/video camera (right).

The Video-Laser System

The Video-Laser System consists of the laser and video camera (Fig. 3). It contains a 3-Alpha laser altimeter, manufactured by Optech Inc., which is used to

measure flying height, ice roughness and laser intensity; for a sampling rate of 30 Hz it provides a 1.5m sample spacing for a flying speed of 80 knots. The digital camera used is an Axis 210 manufactured by Axis Communications. Images are typically collected at a rate of 2 Hz, but the rate is determined by the logging system based on the image field of view, flying height and speed. Each image is 640 by 480 pixels in size, and with a typical flying altitude of 90 m, each pixel is approximately 30 cm by 30 cm in size. For quick reference, the width of the video frame image equals 1.1 times the height of the video camera above the pack ice surface.

The purpose of the Video-Sensor system is to provide 2-dimensional visual information of the ice cover properties. It provides data on lead and ridge distributions and orientations, and on floe size distributions along the flight path of the helicopter. It complements the one-dimensional line profile data of the "Ice Pic" sea ice thickness sensor (Prinsenberg et al., 2002). As the "Ice Pic" sensor includes any snow in its sea ice thickness measurement, a separate measurement of the snow thickness layer is required to get an accurate ice-only measurement. This has lead to the addition of a GPR to the Video-Sensor System to measure snow thickness.

The helicopter needs to fly low (altitude 4 to 6m) when logging GPR and EM data, so digital video images are not recorded during these survey lines. The Video-Sensor system also collects laser altimeter for additional surface roughness determination. Normally along return flights to fuel depots, Video data were collected at an altitude of approximately 90-100m.

GPS Sensors

Both the "Ice Pic" and GPR/Video systems have their own GPS sensors so that the systems can be flown independently of each other when either malfunctions. The systems no longer rely on the helicopter GPS sensor as was the case in the past. The GPS units used are Garmin GPS18's made by Garmin International Inc., Olathe, USA. The GPSs include an embedded receiver and an antenna, and track up to 12 satellites at a time, while providing fast time-to-first-fix, precise navigation updates once per second. The units are designed to withstand rugged operations, are waterproof and require minimal additional components to be supplied by a system integrator. The "Ice Pic" and Video systems provide the GPSs with a source of power, and a clear view of the GPS satellites is required. Listed position accuracy are given as <15m, 95% of the time.

Survey Description

After arriving in Inuvik late Monday March 29, time was available only to check if all the equipment was there and meet the pilot Corey Arsenault. It took most of the following day, Tuesday March 30, to unpack the instrumentation and mount the systems on the helicopter. Late Wednesday morning, the system was test-flown locally over the Mackenzie River, to check out all the systems and to provide the pilot some time to gain experience in low-level flights. Corey went over the safety features and restrictions of low-level flights. One problem emerged: no passenger will be allowed in the front passenger seat, and only personnel required to operate the equipment will be allowed on

board when data is collected during low-level surveying. This meant that no wild-life observer could come along during our survey. This was discussed with James Pokiak of the Tuktoyaktuk Hunters and Trackers Committee (HTC), who had to go back to the Tuktoyaktuk HTC to report and discuss this. Thanks to James Pokiak, we were given permission to go ahead after several phone calls. It also turned out that we would work through the Easter weekend which is a major family social event throughout the North. Below is a summary of the survey data acquisition. A complete day-to day report on the daily survey tasks and results are listed in the Appendix 2.

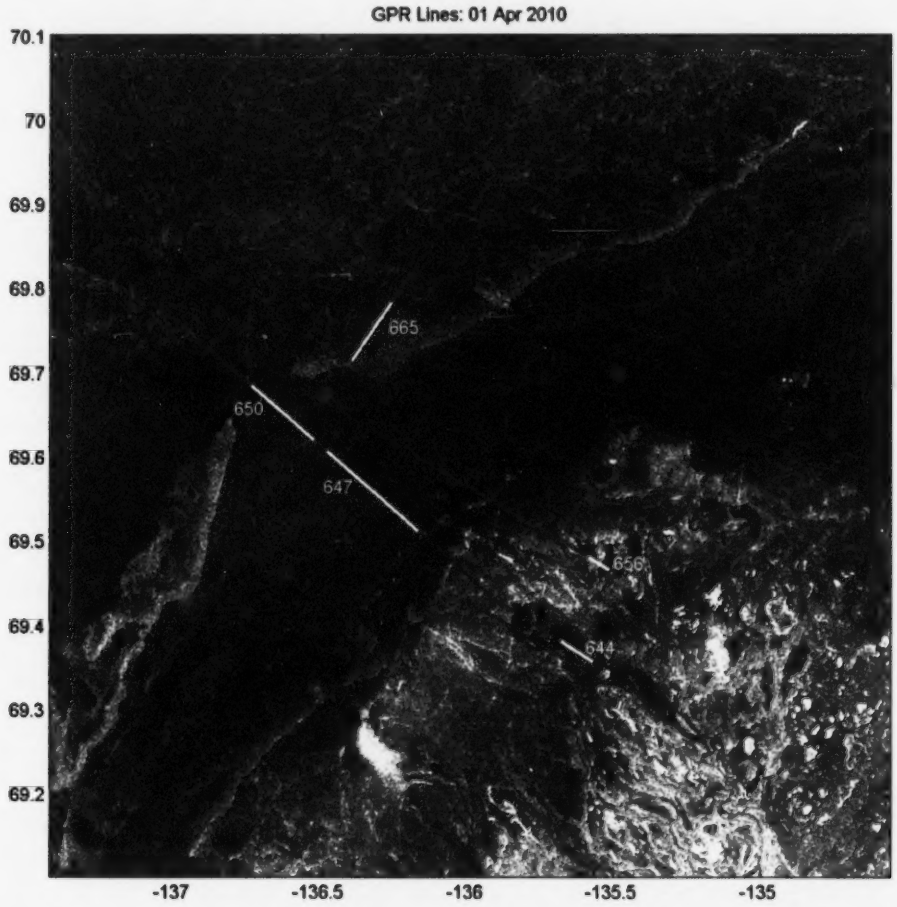

Fig. 4 GPR data line sections flown on April 1 overlain on a RADARSAT-2 SAR image of April 3 (© RADARSAT-2 Data and Products © MacDonald, Dettwiler and Associates Ltd. (2010) - All Rights Reserved).

On the morning of Thursday April 1, the weather over the pack ice was marginal, but expected to clear throughout the day. This delayed our departure to 10:00. After topping up on fuel at Swimming Point, the flight line from Stns. 15 to 16 and 17 was surveyed at low altitude on the way out to collect EM/GPR data, and surveyed back at 100m altitude to collect Video data. Stn. 17, the offshore station is where H. Melling of IOS had deployed a year-long mooring. As shown later in "Data Samples" section, very

rough, ridged mobile ice was present over the mooring site. Next, the line between Stns. 19 and 18 was surveyed; again EM/GPR data were collected on the way out and video data on the way back. After completion of the line, we returned to Swimming Point for fuel. In the afternoon (14:45) an L-shaped flight line was surveyed. Starting at Stn. 5, the survey line went offshore to Stn. 2 and then turned NE to Stn. 3. EM/GPR data were collected on the way out and video data on the way back. This completed the surveying of the first day, and after stopping at Swimming Point for fuel (16:45), we returned to Inuvik. The flight lines for April 1 with GPR file numbers are shown in Fig. 4.

During the first day of the survey, a large dataset was collected; this fact became important as the next three days turned into weather days (when flying was not possible due to bad weather). Normally, weather delays account for 30% of the total time during Arctic winter-spring surveys. This long delay was worrisome, but provided time to look at the data and fine-tune the priorities of the remaining work for the final 6 days, keeping in mind the early spring-type weather that was occurring. Finally on April 5, the weather cleared over the western Delta, and survey day #2 started with the plan to collect more lines in the area previously visited on April 1.

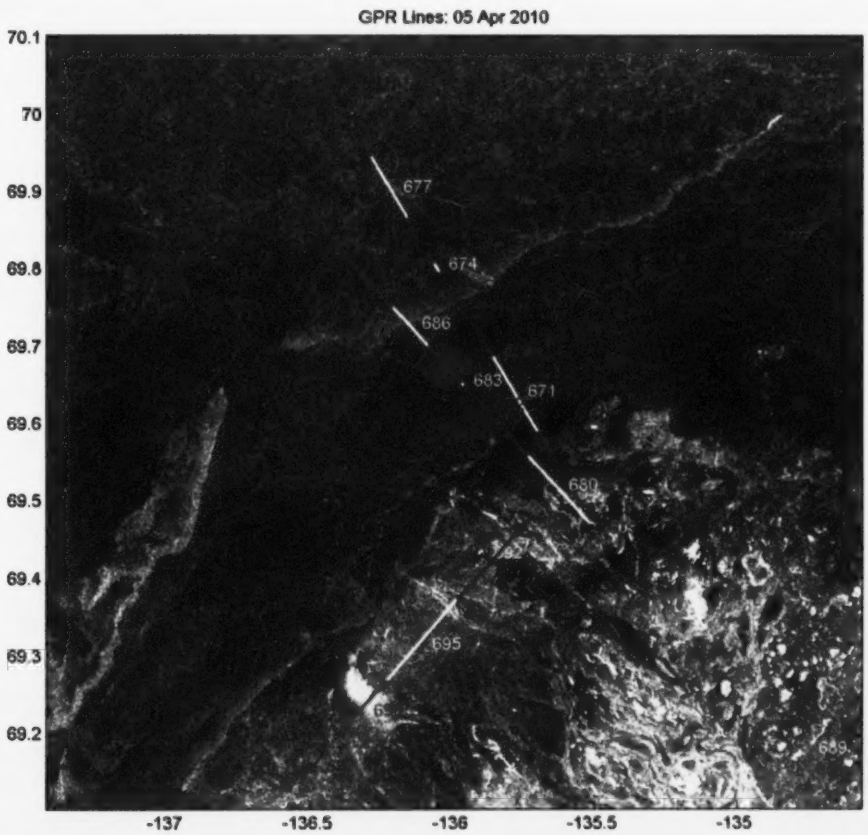

Fig. 5 GPR data line sections flown on April 5 overlain on a RADARSAT-2 SAR image of April 3 (© RADARSAT-2 Data and Products © MacDonald, Dettwiler and Associates Ltd. (2010) - All Rights Reserved).

After fuelling up at Swimming Point, EM/GPR data were collect along a line to Stn. 27, that ended over the rubble field of Tarsiut. After completing the EM/GPR line at 11:30, Video data were collected along a closely-spaced grid over Tarsiut itself, even though the weather was overcast and the video data would not be of the highest quality. However looking at the days we had lost so far, it was decided to do it while we were in the area, as it may have been the only opportunity. After completion of the grid survey over Tarsiut, video data were collected on the way back to Swimming Point for fuel via Stns. 26 and 5 (12:45). After re-fuelling, EM/GPR data were collected along the line from Stn. 5 to Stn. 42, on the way to doing the video grid work over the second rubble field, Minuk (Stn. 25). Weather was better but still overcast. The parallel video grid lines flown over Minuk (Stn. 25) were flown at 100 degrees to the east. After completion of the rubble field survey, video data were collected on the way to Swimming Point (16:00) via Stns. 25, 42 and 5. There was enough time before returning to Inuvik to do the shallow inshore W-E line between Stns. 21 and 20, after repeating the EM/GPR short line between Stns. 19 and 18 (see Fig. 1 for station numbers). Fig. 5 shows the survey lines collected on April 5 highlighting the GPR line sections.

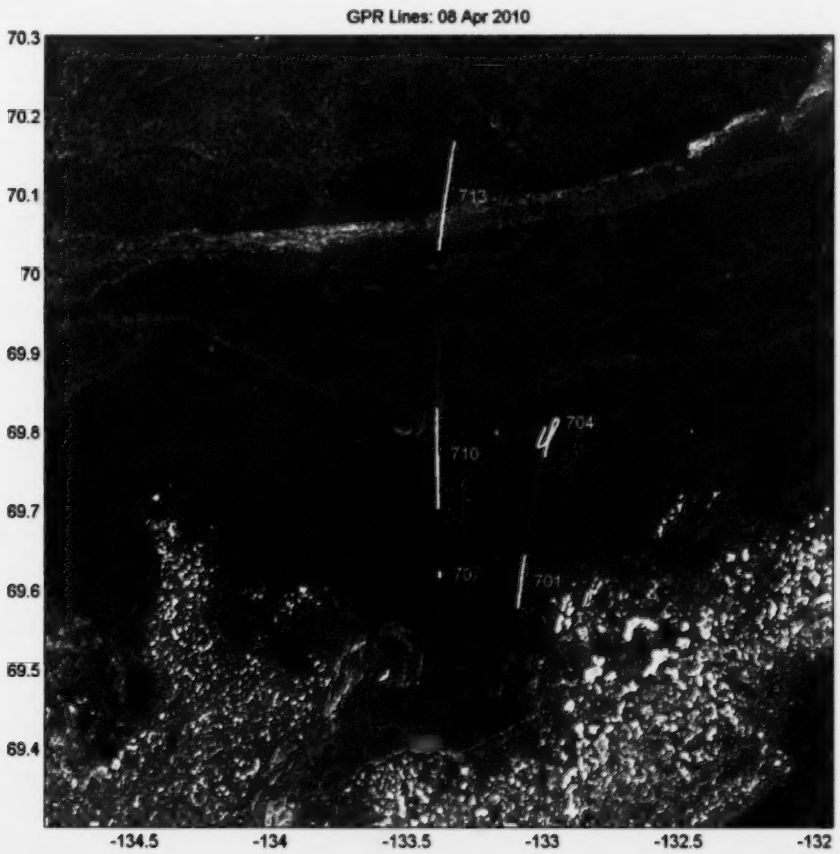

Fig. 6 GPR data line sections flown on April 8 overlain on a RADARSAT-2 SAR image of April 3 (© RADARSAT-2 Data and Products © MacDonald, Dettwiler and Associates Ltd. (2010) - All Rights Reserved).

April 6 and 7 were also weather days, which further restricted the airborne and on-ice survey work. Most of the promised work to the other PERD project managers of IOS, NRC and GSC were completed. On April 8, the weather cleared in the afternoon and two helicopters were used to do both the airborne and on-ice sampling work. The on-ice work with pilot Corey Arsenault was planned for 5 stations along the "L" shaped line flown on April 1 (Fig. 4). The airborne survey with pilot Jory Bott would collect EM/GPR and Video data along the N-S line and inshore "L" shaped line north of Tuktoyaktuk (Fig. 1). The on-ice survey did the work as planned; shallow CTD profiles, snow depths, ice thicknesses through ice-augered holes and ice chip samples were collected. The data are listed in Table 2 in the "Data Sample" section. More on-ice work was planned, but could not be accomplished due to the weather delays. The second helicopter collected EM/GPR data along the line section anchored by Stns. 24, 23 and 29; Stn. 29 being a TerraSAR-X Super Test Site where high resolution satellite X-band SAR data were collected. A parallel grid line pattern was flown over this location collecting both EM/GPR data and Video data before returning to Tuktoyaktuk for fuel (16:30). After obtaining fuel, the N-S line was surveyed for EM/GPR data on the way out and for Video data on way back, before returning to Swimming Point for fuel (18:30). There was not enough time left to repeat the Video grid lines of Tarsiut and Minuk rubble fields; thus we returned to Inuvik. Fig. 6 shows the survey lines flown on April 8 north of Tuktoyaktuk.

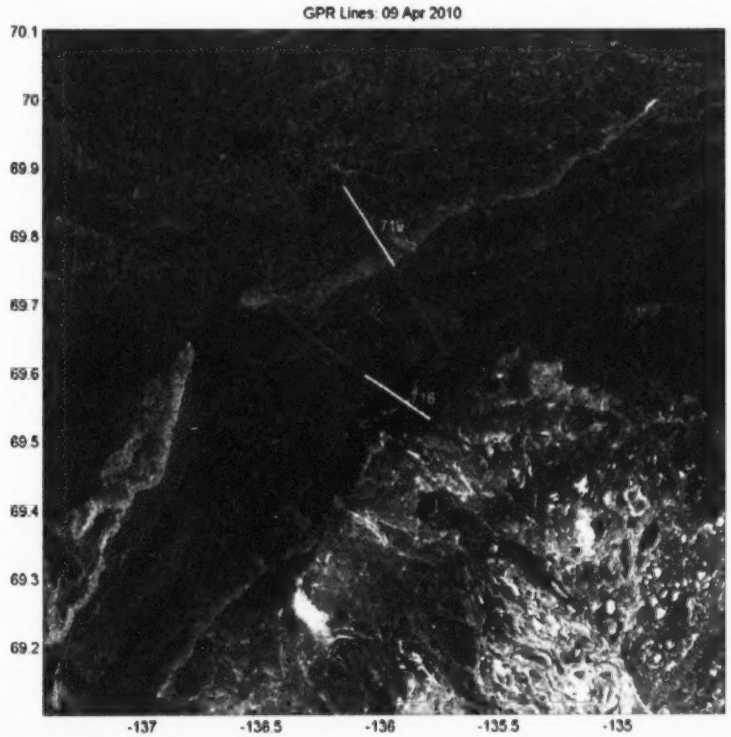

Fig. 7 GPR data line sections flown on April 9 overlain on a RADARSAT-2 SAR image of April 3 (© RADARSAT-2 Data and Products © MacDonald, Dettwiler and Associates Ltd. (2010) - All Rights Reserved).

With a good weather forecast for the following day, the survey was extended by one day in order to repeat the video data collection of the Tarsiut and Minuk rubble fields. While packing other on-ice instrumentation during the morning of April 9, a triangle anchored by the two rubble fields (Stn. 25 and Stn. 27) was surveyed. After fuelling up at Swimming Point (10:00), EM-GPR data was collected between Stns. 5 and 25, parallel video grid lines were then flown over Minuk (Stn. 25) followed by another set of video grid lines over Tarsiut (Stn. 27) before collecting EM/GPR data on the way back from Stn. 27 to Stn. 5 and returning to Inuvik via Swimming Point. Fig. 7 shows the survey lines flown on April 9. The survey equipment was taken off the 206L helicopter in the afternoon and packed for shipping back to Bedford Institute of Oceanography.

Data Samples

In this section we will display samples collected during the 2010 Beaufort Sea survey. Not all the data will be shown, but can be found on the DFO Maritimes FTP site: ftp://starfish.mar.dfo-mpo.gc.ca/pub/ocean/seaice/.

Data plots from April 1 will mainly be shown; their flight paths were shown in Fig. 4. The height flown along this "L-shaped" line is shown as a time series profile plot of the "Ice Pic" laser (Fig. 8). The laser plot shows the high altitude return loops at regular intervals (8-10 minutes) during which background EM data were obtained in order to remove EM baseline drift. They are collected both along the flight path, and at the start and end of the survey line. During these "EM back-grounds" at 400ft, the GPR collection was stopped, thus breaking up the GPR into the sub-sections data files as shown in Fig. 4. The EM and GPR data files of the total survey are listed in Table 1.

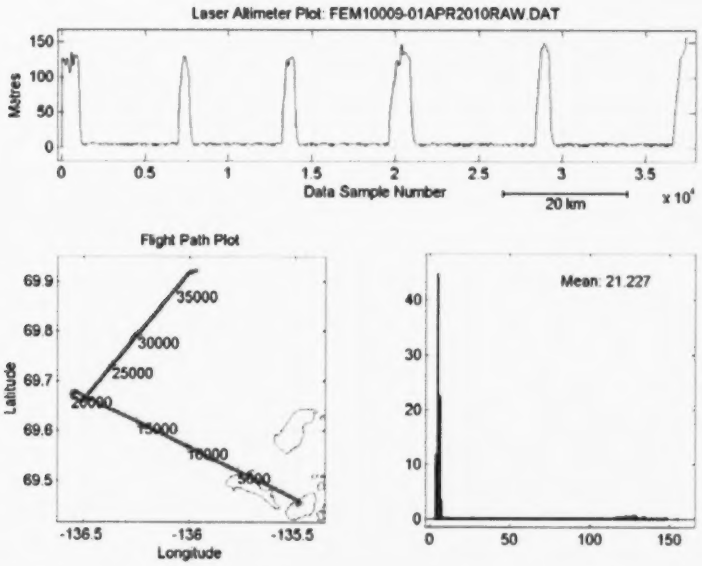

Fig. 8 Laser time series profile of the survey line between Stns. 5, 2 and 3.

EM Data

Ice thickness and conductivity is computed from the EM data by an inversion program running on the logging PC in the helicopter, and is shown in real-time on the operator's display monitor to ensure data are being logged. The real-time inversion program uses a model with a constant value of 2.5 S/m for the lower layer (seawater) conductivity, and the upper layer (sea ice) conductivity is allowed to vary. However, for most of the area sampled over the Mackenzie shelf, the conductivity of the oceanic surface layer is much lower and often indistinguishable from that of the overlying ice, because of freshwater input from the Mackenzie River. Therefore in the post-processing inversion program, the conductivity of the bottom layer (brackish water or sediment) is allowed to vary, and the conductivity of the upper layer (ice and/or freshwater) is set to 0.0 S/m. On the FTP site, "Quick-look" plots of the ice thickness profiles are available for the total flight paths and for sub-sections, as shown in Figs. 9 and 10. Plots are available for both the real-time and post-processing inversion programs.

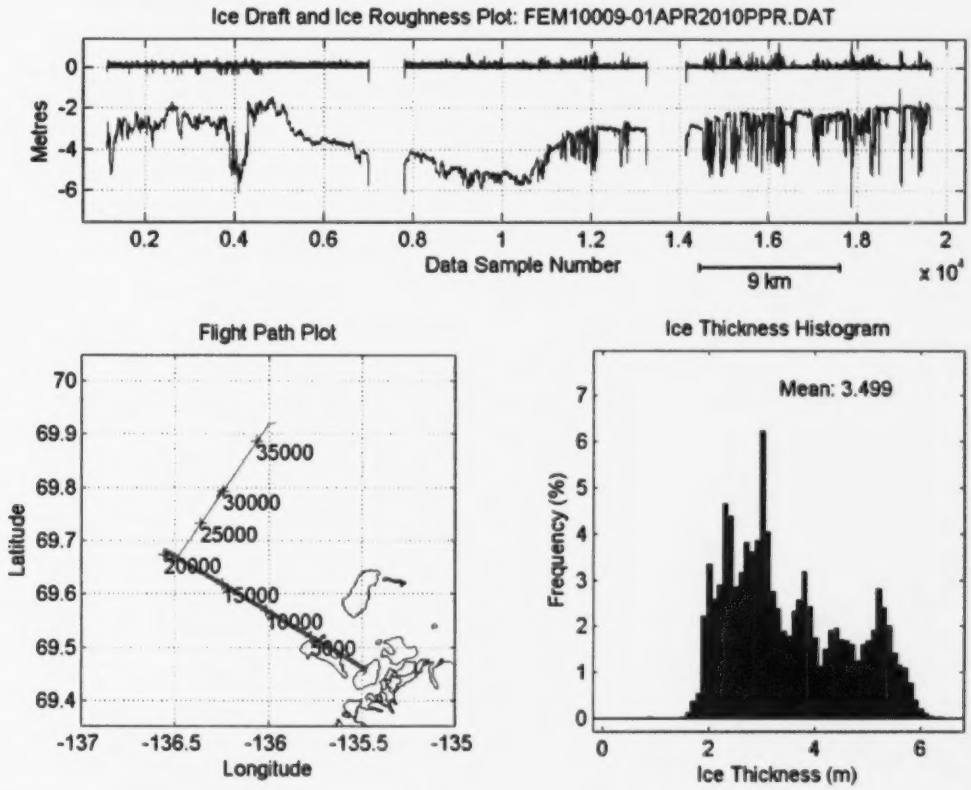

Fig. 9 Ice thickness and ice roughness "Quick-look" profile plot for the line section between Stns. 5 and 2, collected on the afternoon of April 1.

Apparent ice thickness profile data are shown for the line section (green line) from Stn. 5 to Stn. 2 in Fig. 9, and for the line section between Stns. 2 and 3 in Fig. 10. These plots show the pack ice roughness from the laser data plotted upward, and the depth of the top of the lower (conductive) layer from the EM data plotted downward. Fig. 9 shows three data sub-sections; the inshore section is in a very shallow region where freshwater is found. The ice draft corresponds to the water depth over unfrozen sediment, and to greater depths over frozen sediment (as at data sample number $0.4x10^4$) and infers large "ice thicknesses" as no clear ice-sediment layer interface is present. For floating ice on low salinity inshore waters, the lower layer represents the bottom sediment. Once the sediment is frozen and attached to the ice, it represents part of the upper layer in the inversion model, since the conductivity of frozen sediment is similar to that of ice (about 0 S/m).

At the end of the first sub-section, the bottom depth is four meters. The apparent ice draft represents the total water depth in the first part of the second sub-section, however it then represents the depth of the freshwater plume, above a more conductive saltwater layer, with ice keels sticking through in places (sample number $1.2x10^4$). In the third sub-section, rough ice at sample number $1.65x10^4$ is trapping water of the freshwater plume inshore to a depth of 3m. The laser surface roughness is highly coherent with the rough ice rubble keel features. The rubble field at sample number $2.4x10^4$ in the second line section (Fig. 10) is the last ridge that appears to hold back the freshwater plume (depth 2.1m) with level ice thicknesses past the ridge of around 1.6m. Also some leads with thinner ice can be seen and are discussed later.

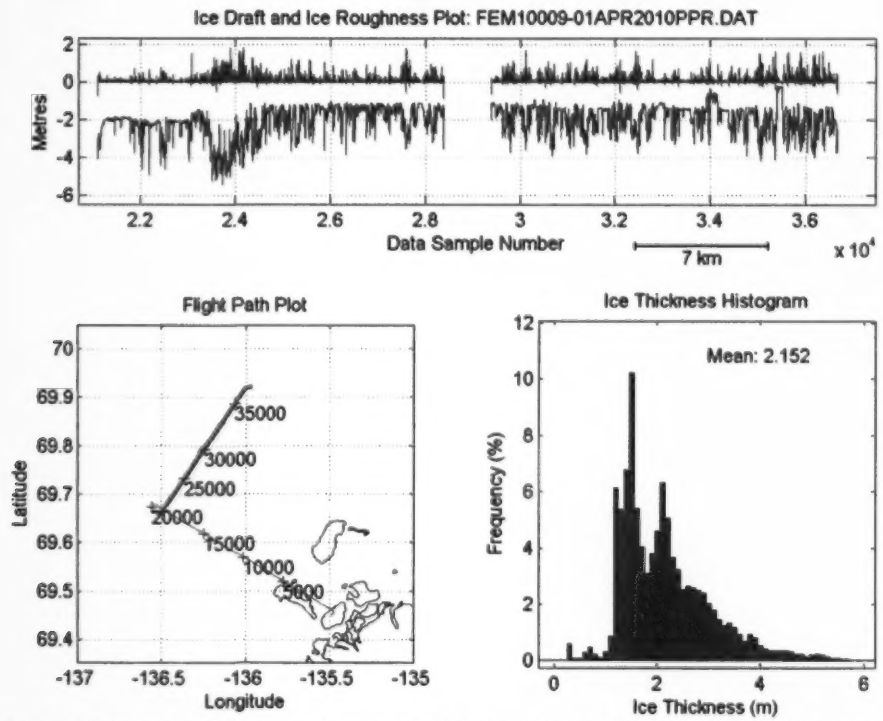

Fig. 10 Ice thickness and ice roughness "Quick-look" profile plot for the line section between Stns. 2 and 3 collected on the afternoon of April 1.

At the end of the morning flight of April 1 (FEM10003), the ice was rough and ridged where the IOS mooring was located (Stn. 17), yet on either side of the site (SE and NW), very homogeneous flat ice sections were seen (Fig. 11). The area was part of the mobile offshore, as fresh narrow leads were observed.

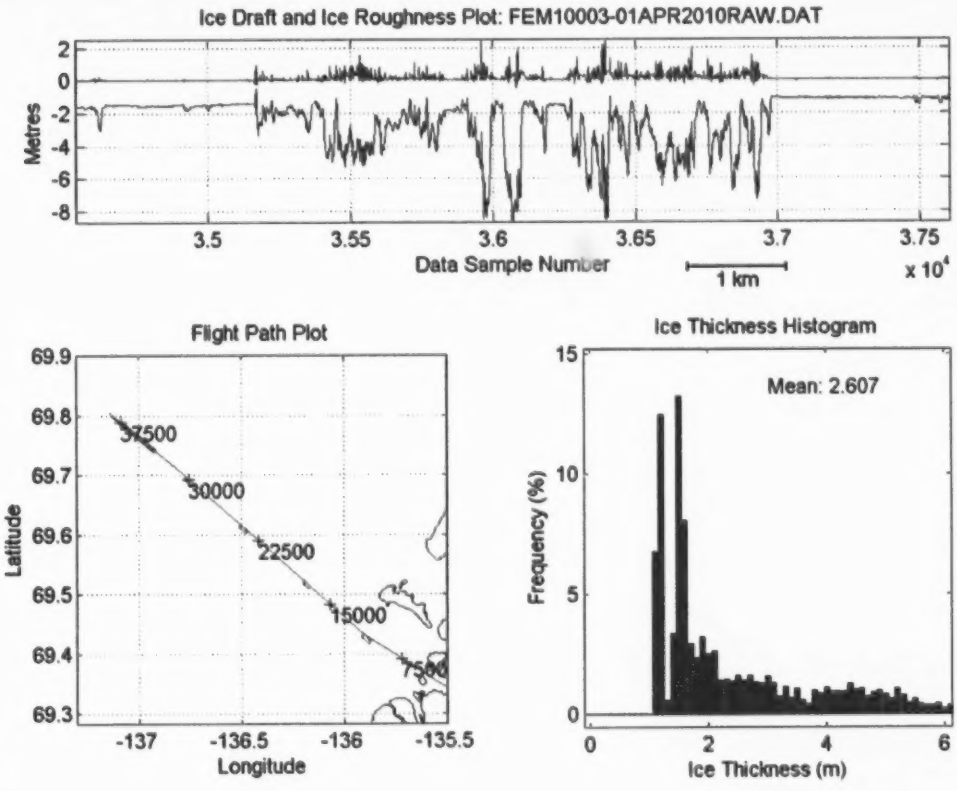

Fig. 11 Ice thickness plot of the sub-section covering the mobile ice near Stn. 17 where the IOS mooring is located.

On the DFO-Maritimes FTP site, EM data are stored as files and plots. The files collected in the helicopter are the "PIC rawfiles". Data from the "rawfiles" are extracted into the "PIC datfiles", which are used in the field to quickly plot the observations as line plots and histograms. The plots are e-mailed to other collaborators and Canadian Ice Service for their inclusion in the production of ice charts. During the transcribing of the RAW files into DAT files, ASCII data files (*.IPP) are also generated and used in additional analysis and plotting. These files are all on the FTP site along with the "IcePic dat" plots that can be accessed through the DFO Maritimes "Seaice Website". http://www.mar.dfo-mpo.gc.ca/science/ocean/seaice/public.html and the Seaice Website's data link: ftp://starfish.mar.dfo-mpo.gc.ca/pub/ocean/seaice/.

Table 1 below shows the EM and GPR data files collected during the Beaufort Sea ice survey in April 2010. It lists the files numbers and the stations linking the total flight line in sequential order. The station locations are shown on Fig. 1 and their latitude and longitude are listed in Appendix 1. The approximate time in Mountain Daylight time is listed for each GPR subsections.

Table 1: Mackenzie Delta 2010 GPR and EM files

Day	JDay	~ Time	GPR File #	Stns	EM file #
Mar 31	90-1		----------	River	1002
April 1	91-1	11:48	F643 - F645	15-16-17	1003
		11:55 - 12:08	F646 - F647	15-16-17	1003
		12:17 - 12:29	F649 - F652	15-16-17	1003
		13:17 - 13:34	F654 - F655	19-18	1006
		Fuel Depot			
April 1	91-2	14:50 - 15:20	F656 - F662	5-2-3	1009
		15:20 - 15:55	F663 - F667	5-2-3	1009
April 5	95-1	10:43 - 11:23	F668 - F677	5-26-27	1011
		Fuel Depot			
April 5	95-2	13:30 - 14:30	F679 - F688	5-42-25	1013
		14:35	No GPR	42-25	1015
		Fuel Depot			
April 5	95-3	16:25 - 17:35	F690 - F697	15-16-21-20	1018
April 8	98-1	15:02 - 15:20	F699 - F700	24-23	1020
		15:23 - 15:59	F701 - F704	23-29 and 29	1020
		Fuel Tuk			
April 8	98-2	17:07 - 18:05	F705 - F713	10-11	1021
April 9	99-1	11:04 - 12:08	F715 - F718	5-25	1022
	99-2	13:08 - 13:19	F719 - F723	27-5	1022

EM files 1008 and 1019 are test files over land areas

GPR Data

Since the collection of GPR data is very new, the processing and display of the data in the field and used in this report are not as far advanced as the EM data collection and analysis routines. The GPR data and plots on the FTP site are for now stored as GPR data files (GPR Raw and GPR GPS files) and as GPR processed files that are used in further analysis and as GPR time series plots. The plots shown below and stored on the FTP site have been screen-grabbed while running the display software, also used for checking the data quality in real-time collection mode. A quick-look plot of the raw GPR data from line section F656 is shown in Fig. 12 with scan number along the x-axis

(approximately 1 scan per 1.0 to 1.5m traveled) and the vertical sample numbers increasing down along the y-axis indicating the distance from the helicopter GPR sensor. The top light echo is the distance to the snow-air interface, and thus is the height of the helicopter. The middle dark echo is the snow-ice interface. A dark bottom echo indicates the bottom of the ice, overlying water, and a light-toned echo indicates the bottom of ice overlying frozen sediment (in a bottom-fast ice (BFI) area). The data shown in Fig. 12 were collected from a very shallow area (2-3m water depth) as shown on the line plot of Fig. 4. Figure 4 shows that bottom-fast ice areas were present at both ends of the plot, with floating ice in between. This is in agreement with the SAR data in Fig. 4, which shows dark BFI areas at both ends of the flight line.

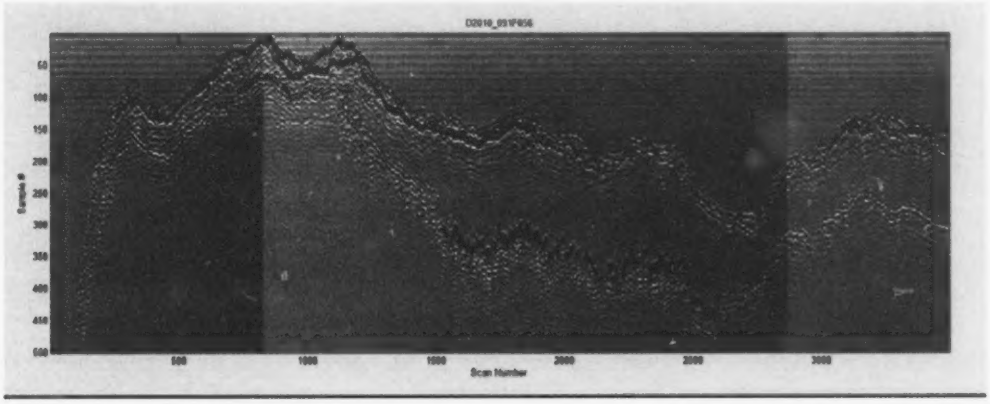

Fig. 12 Quick-look GPR time series plot of line sub-section F656 of April 1; it covers about 4km along the horizontal axis and about 6m along the vertical axis.

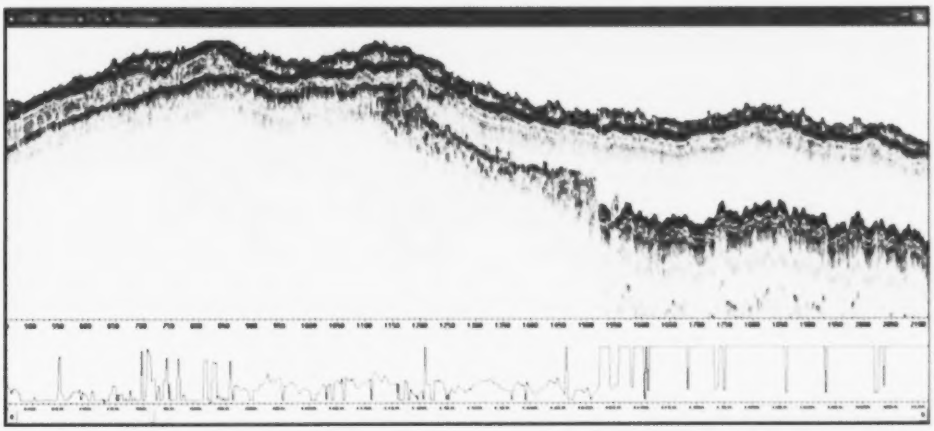

Fig. 13 High resolution display of GPR data for a F656 sub-section collected in the afternoon of April 1. Snow depths up to 1m are plotted along the bottom panel but only represent true snow depths when the third bottom echo is weak or absent.

Fig. 13 shows more details of F656 (Fig. 12) by a "screen-grab" plot made from the display software. The GPR echo plot displays echos vertically, 3.5m to 10.5m below

the helicopter sensor between scan #500 to #2000 in Fig. 12, covering about 2km along the horizontal axis. Ice thicknesses of about 1-1½ m can clearly be seen from sample 1550 onwards. Before this, the ice-bottom echo is weaker, indicating the ice, less than 1m, is frozen to and possibly into the low salinity bottom sediment layer. Over the entire profile, the software is able to extract snow depths (bottom panel), at places reaching 40cm of the total possible display height of 1m.

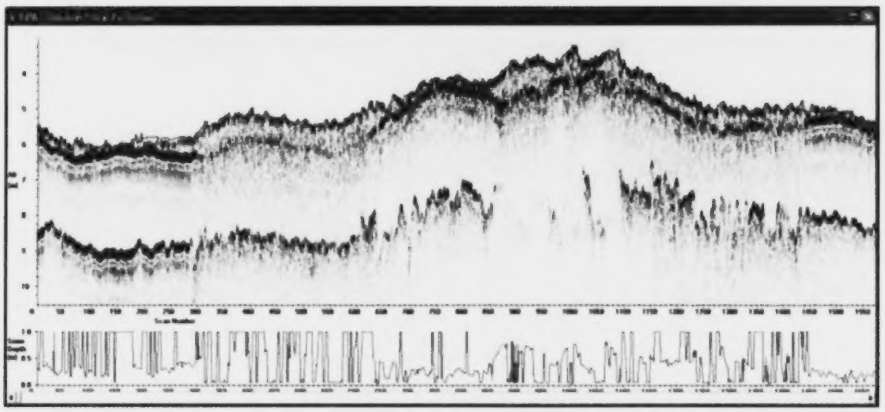

Fig. 14 First part of the GPR section F660 passing over a major rubble area (#1000), where very deep snow accumulated in the rough surface ice topography. The vertical scale in the top panel provides the height with respect to the propagation of radar waves in air, and thus overestimates the snow and ice thickness.

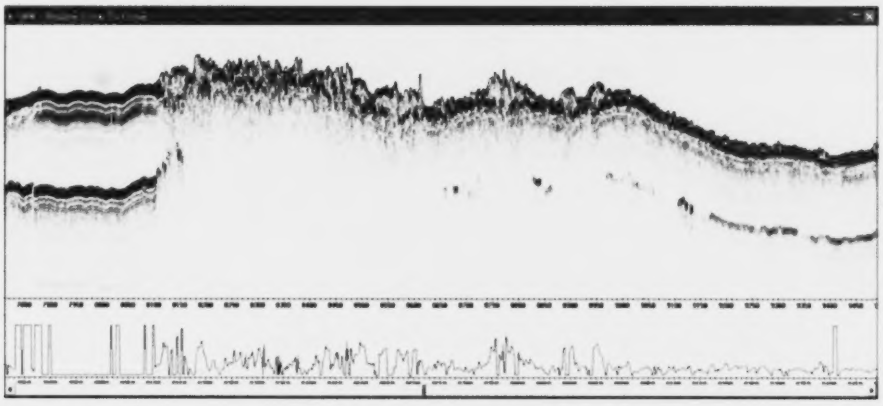

Fig. 15 Offshore part of the GPR section F660 passing over another rubble field, beyond which the GPR starts losing the bottom ice echo due to increased brine volume.

Figs. 14 and 15 show GPR components of the GPR section F660. Both show rubble fields where snow is trapped in the rough ice topography and where the GPR does not record a bottom ice echo, because of increased ice salinity reducing GPR penetration. Level ice thicknesses of ~1-1½ m are shown on either side of the rubble fields. Offshore of the rubble field shown in Fig. 15 (water depth ~5m), the GPR starts losing the bottom ice echo as the ice brine volume has increased and at the same time the EM (Fig. 9) starts

to record saltwater conditions below the freshwater plume layer. Starting along the GPR section F661 (Fig. 16), the bottom ice echo is just visible before it disappears when entering the rough and thick ice shown by the EM plot at sample number 1.45×10^4 (Fig. 9).

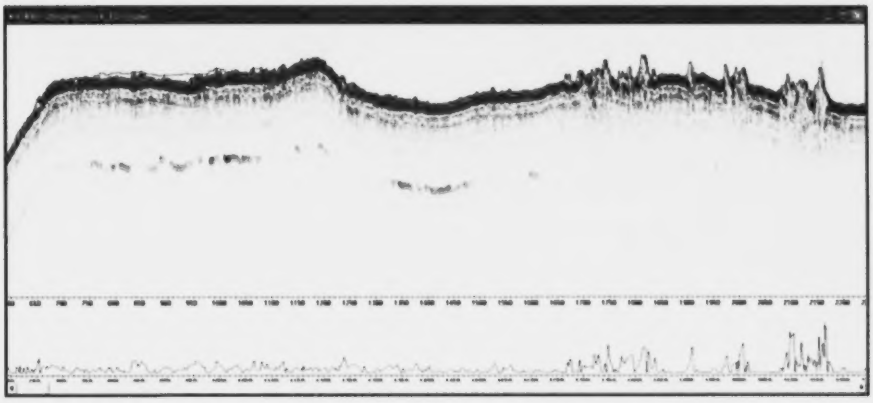

Fig. 16 Start of GPR section F661 showing the faint bottom ice echo and then the start of the rough ice topography (#1700). Very little snow is present over the flat ice.

Post-processing software for the GPR data is being developed to generate line profile plots and histograms similar to that developed for the EM ice thickness data. An example of the post-processing of GPR data is shown below when both snow depths and ice thickness are available. Other examples of post-processing GPR data are shown in Appendix 3.

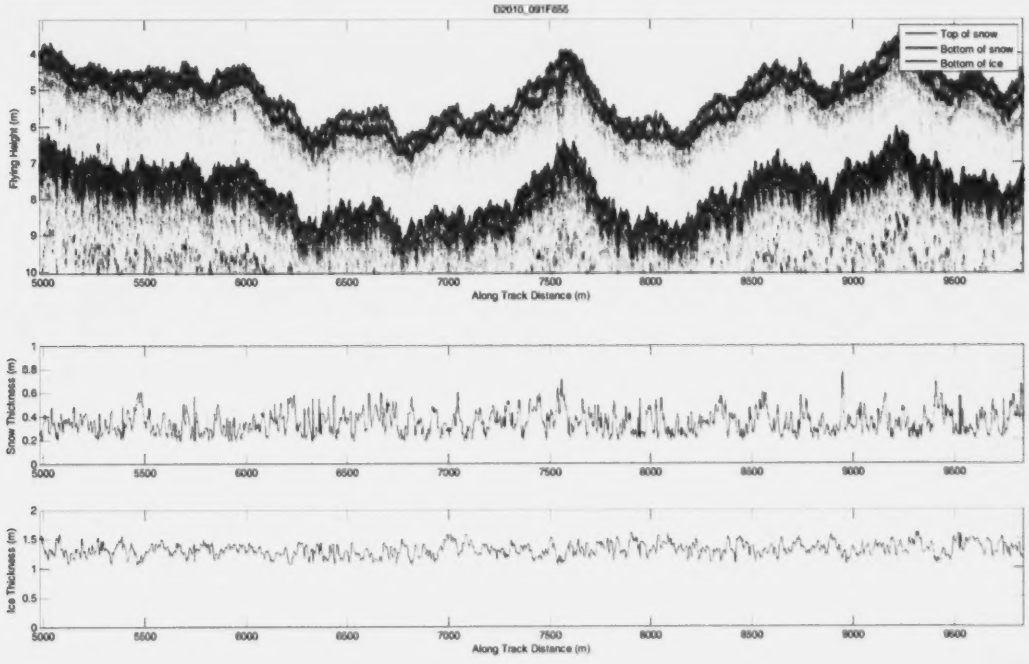

Fig. 17 GPR section from F655 (~5km) showing the GPR data and annotated colour lines denoting the top of the snow layer (green line), the bottom of the snow layer (red line) and the bottom of the ice cover (turquoise line). The resulting snow depth and ice thickness profiles are shown in the lower panels. The vertical scale in the top panel provides the height with respect to the propagation of radar waves in air, and thus overestimates the snow and ice thickness.

Video Data

Video data were normally collected on the way back along the same flight line as EM-GPR data were collected on the way out (offshore). Table 2 lists the video file numbers, time of recording and the area they were collected (station numbers).

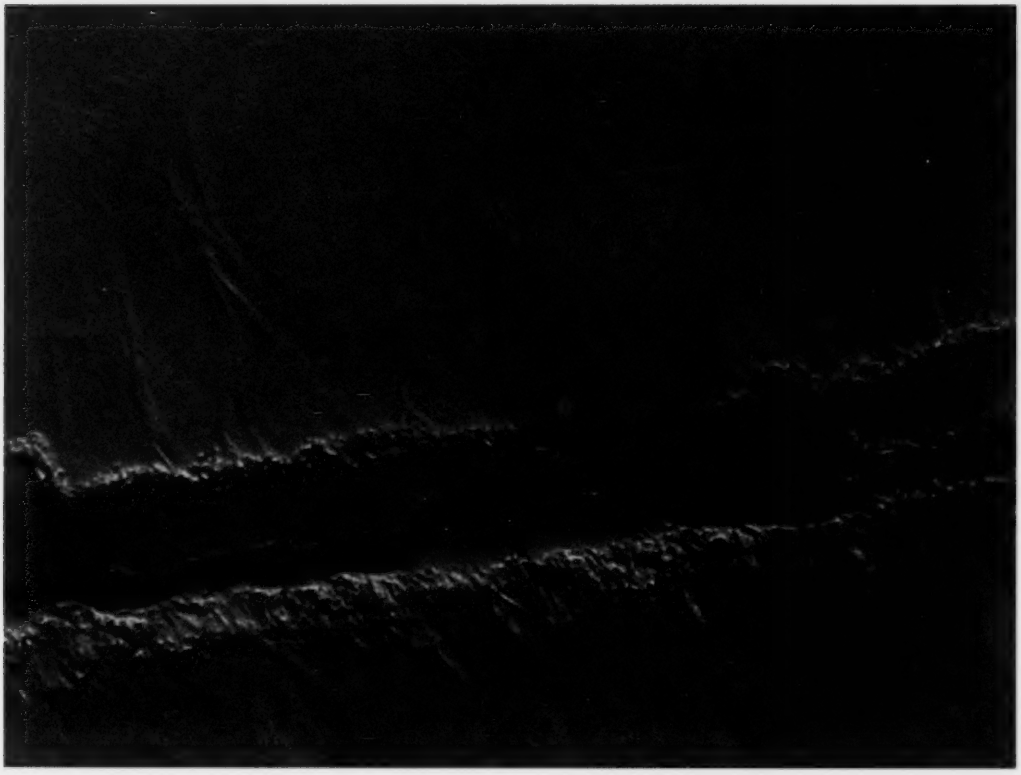

Fig. 18 Video image of the small lead passed over on April 1 from Stn. 17 to Stn. 16, frame #6518. The middle, right of the image is unclear due some water on the outside lens cover.

The EM system logs the GPS track (File number also listed in Table 2) and provides a GPS/time back-up file even though the Video system has its own GPS and laser. Video frames are collected at approximately 90-100m altitude and at a rate that assures an overlap of 40% between frames. The frame interval to accomplish this is determined by the system using the GPS height and helicopter ground speed. Each

individual frame has its own lat/long, height of camera and collection time that can be generated through a program "Image Web Page" using the stored video data files. Mosaics a can be generated through another program called "Video System Viewer", both linear quick-look mosaics, and geo-corrected mosaics can be generated. For the latter, it is usually preferable to select a small data set of ~10 frames for the features to be easily visible.

Table 2: Mackenzie Delta 2010 Video and EM-Laser files

Day	JDay	~ Time	Video File #	Stns	EM file #
April 1	91-1	14:23*-11:35	F025 - F026	to 15	-------
		12:41 - 13:17	F027 - F030	17-16-15	1004, 05
		13:33 - 13:43	F031	18-19	1007
		Fuel Depot			
April 1	91-2	14:45	F032	To 5	-------
		16:01 - 16:34	F033 - F036	3-2-5	1010
April 5	95-1	11:28	F037	To Tarsiut	1012
		11:34 - 12:00	F038 - F050	Tarsiut	1012
		12:02 - 12:23	F051 - F053	27-26-5	1012
		Fuel Depot			
April 5	95-2	14:30 - 14:36	F054	42N-42	1014
		14:37 - 15:04	F055 - F065	Minuk	1016
		15:05 - 15:31	F066 - F068	25-42-5	1017
		Fuel Depot			
April 5	95-3	17:33 - 17:41	F069 - F070	21- Inuvik	---------
April 8	98-1	16:03 - 16:30	F071 - F075	29 and 29-23	1020
		Fuel Tuk			
	98-2	17:58 - 18:21	F076 - F078	11-10	1021
April 9	99-1	12:10 - 12:26	F079 - F086	Tarsiut	1022
		12:26 - 12:34	F087	25 - 27	1022
		12:36 - 12:55	F088 - F094	Minuk	1022

*time needs to be reduced by 3hr (Atlantic time versus Mountain time)

On April 1 a small lead was past on the flight out to Stn. 17 at low altitude. It marked the change from the inshore land-fast ice to the offshore mobile ice. It was again passed over at 100m altitude while collecting Video data. Fig. 18 shows the video frame of the small lead at 69.634N and -136.564W at 12:52 MDT. This location can be found by making a quick-look mosaic of the ice region where (and when) the lead was seen (Fig. 19), from which the video frame number can be approximated and found in the individual video frames.

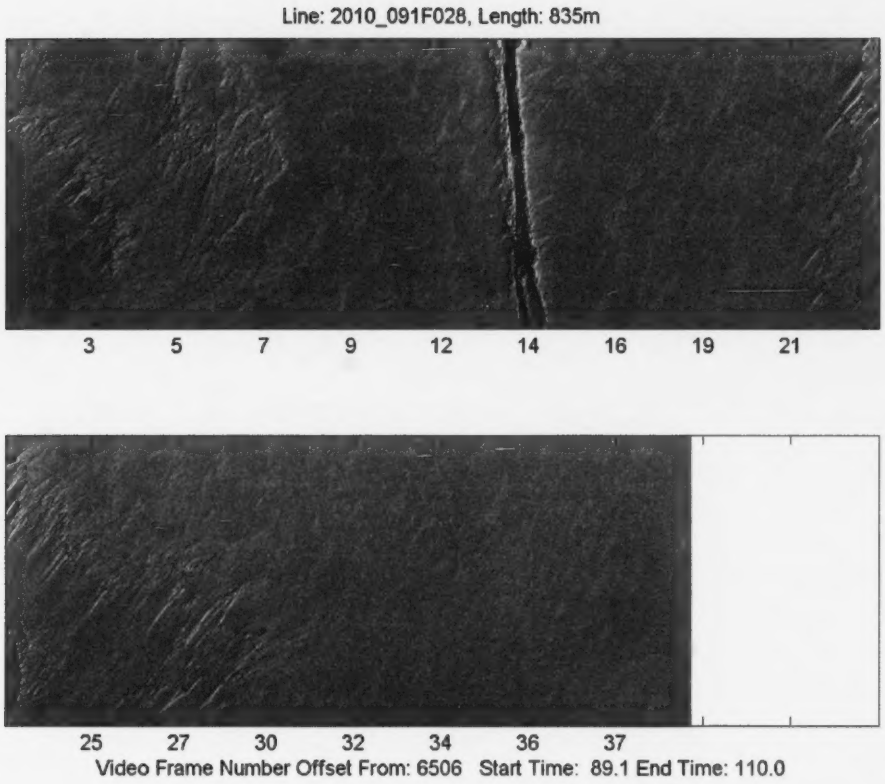
Line: 2010_091F028, Length: 835m
3 5 7 9 12 14 16 19 21
25 27 30 32 34 36 37
Video Frame Number Offset From: 6506 Start Time: 89.1 End Time: 110.0

Fig. 19 Quick-look mosaic of 37 video frames around the start of the 10minute file folder storing the frames collected between 12:50 to 13:00 MDT when the lead shown in Fig. 18 was seen.

Video data were collected twice over the Tarsiut and Minuk rubble fields. Close parallel lines were flown in what was called "race track" grid by the pilots. The lines along which data were collected were in the same direction and a return loop was used to start the next line making the "race track" pattern (Fig. 20). The mosaic for Tarsiut centre line using 10 frames is shown in Fig. 21; it is the trailing or SW end of the rubble field. The mosaic software uses the GPS data and plots in grey scale format. During this survey of rubble fields, laser data were also collected and can be used to form a 3-D roughness map. Since the data are lat/long referenced and the rubble fields are stationary, the laser data of both flights of April 1 and April 9 can be combined.

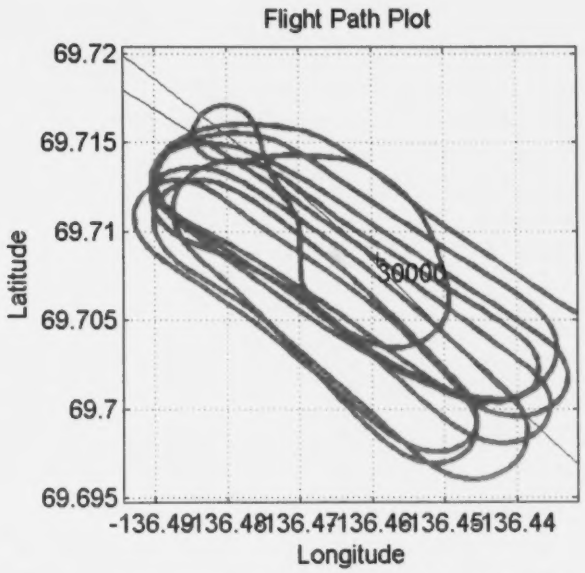

Fig. 20 Mosaic line pattern flown over Minuk rubble field on April 9.

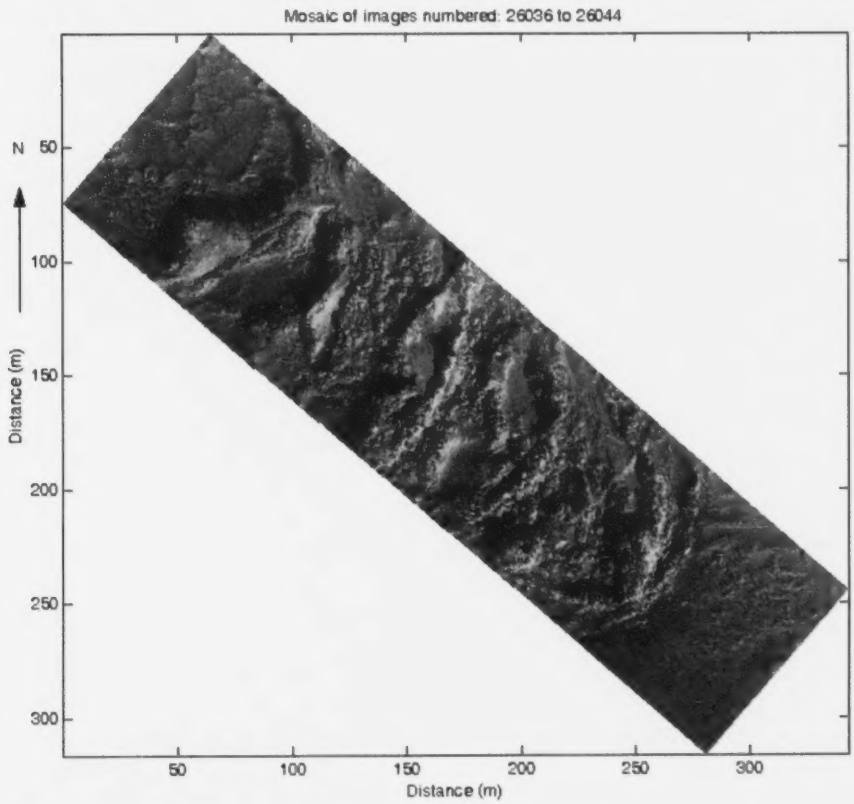

Fig. 21 Mosaic video frames collected over the Tarsiut rubble field on April 9.

The Video frame image locations and camera height at the procurement time can be obtained through a program called "Imagewebpage". It generates a list of all individual images in ten-minute folders where the image numbers are linked to the stored data files and thus can be seen by "clicking" on the image number. A sample of the available files is shown in Table 3 for Julian day 91 file 091F034, GMT hour 6 and the start of the 10-min folder.

Table 3: Section listing of locations and GPS altitude of individual image

V2010-091F034 Hour – 6 Min - 11

i0011397	Lat: 69.71209 Long: -136.40223	GPS Alt: 98.6
i0011398	Lat: 69.71209 Long: -136.40223	GPS Alt: 98.6
i0011399	Lat: 69.71174 Long: -136.40293	GPS Alt: 98.9
i0011400	Lat: 69.71174 Long: -136.40293	GPS Alt: 98.9
i0011401	Lat: 69.71140 Long: -136.40364	GPS Alt: 99.8
i0011402	Lat: 69.71140 Long: -136.40364	GPS Alt: 99.8
i0011403	Lat: 69.71106 Long: -136.40435	GPS Alt: 100.3
i0011404	Lat: 69.71071 Long: -136.40506	GPS Alt: 100.7
i0011405	Lat: 69.71071 Long: -136.40506	GPS Alt: 100.7
i0011406	Lat: 69.71037 Long: -136.40579	GPS Alt: 101.3
i0011407	Lat: 69.71004 Long: -136.40652	GPS Alt: 101.8
i0011408	Lat: 69.71004 Long: -136.40652	GPS Alt: 101.8
i0011409	Lat: 69.70970 Long: -136.40726	GPS Alt: 102.3
i0011410	Lat: 69.70970 Long: -136.40726	GPS Alt: 102.3
i0011411	Lat: 69.70936 Long: -136.40800	GPS Alt: 102.8
i0011412	Lat: 69.70903 Long: -136.40875	GPS Alt: 103.1
i0011413	Lat: 69.70903 Long: -136.40875	GPS Alt: 103.1
i0011414	Lat: 69.70869 Long: -136.40950	GPS Alt: 103.2
i0011415	Lat: 69.70869 Long: -136.40950	GPS Alt: 103.2
i0011416	Lat: 69.70835 Long: -136.41026	GPS Alt: 103.0
i0011417	Lat: 69.70801 Long: -136.41101	GPS Alt: 102.7

On-Ice Data

On-ice data were collected on April 8 using a second helicopter. Five stations along the "L-shaped" flight line flown on April 1 were visited (Fig. 22); their Lat/Long locations are listed in Appendix 1. At each station an Idronaut Ocean Seven 304 CTD was used to collect CTD profiles of the shallow water column along with the collection of ice and snow thickness and ice chip samples.

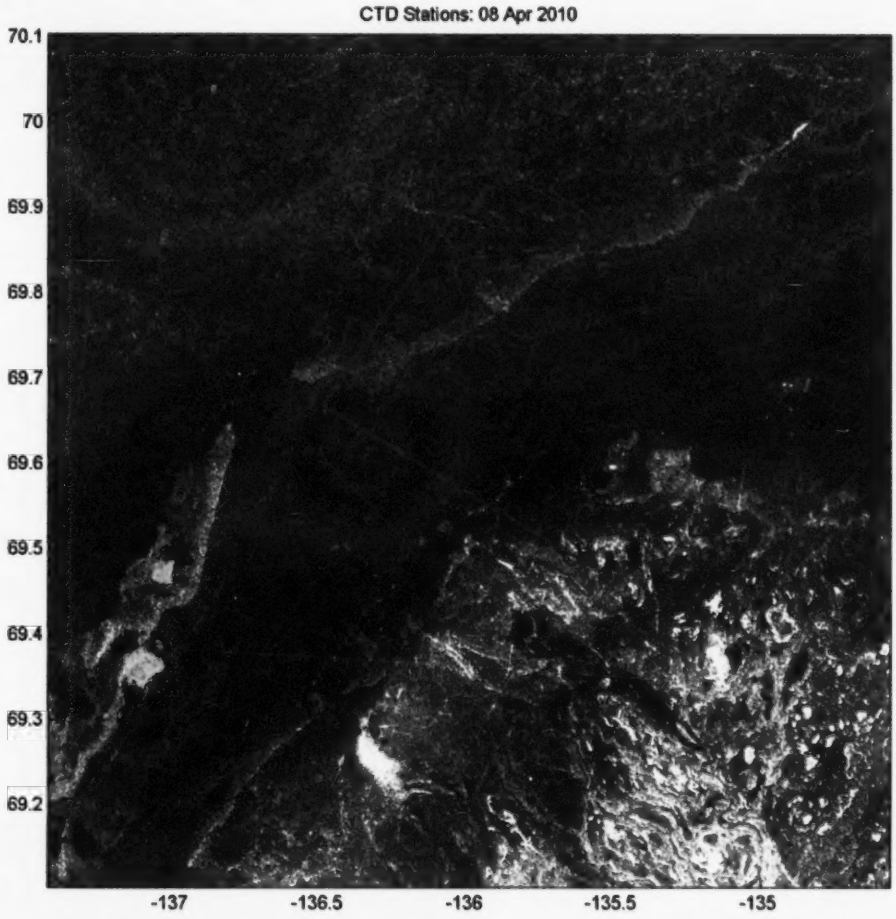

Fig. 22 Location map of on-ice station visited on April 8, 2010. (© RADARSAT-2 Data and Products © MacDonald, Dettwiler and Associates Ltd. (2010) - All Rights Reserved).

The CTD profiles of Stn. 43 (4m water depth) and Stn. 44 (5.5m water depth) did not show any saltwater intrusion, however there were higher salinity values at the bottom of the profiles at Stn. 45 (7m water depth). At Station 46 (Fig. 23), the water depth had increased to 14m and a fresh water plume layer 7m thick with a salinity of 3ppt overlaid the diluted ocean bottom layer (20-25ppt). At Stn. 47 (Fig. 24), the water column over the total depth of 16m was well mixed with a salinity of 30ppt, and no appreciable freshwater plume layer was observed.

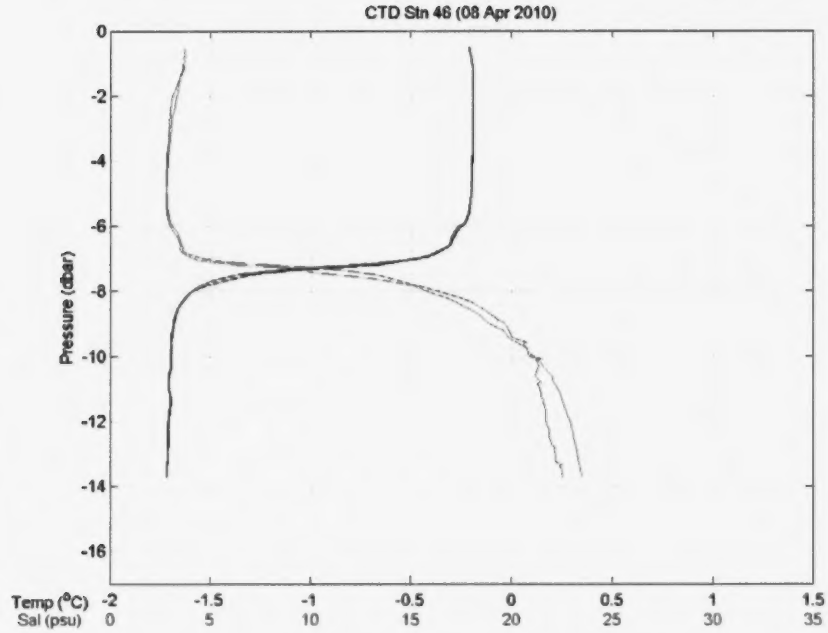

Fig. 23 Salinity-temperature profile of Stn. 46 from April 8, 2010.

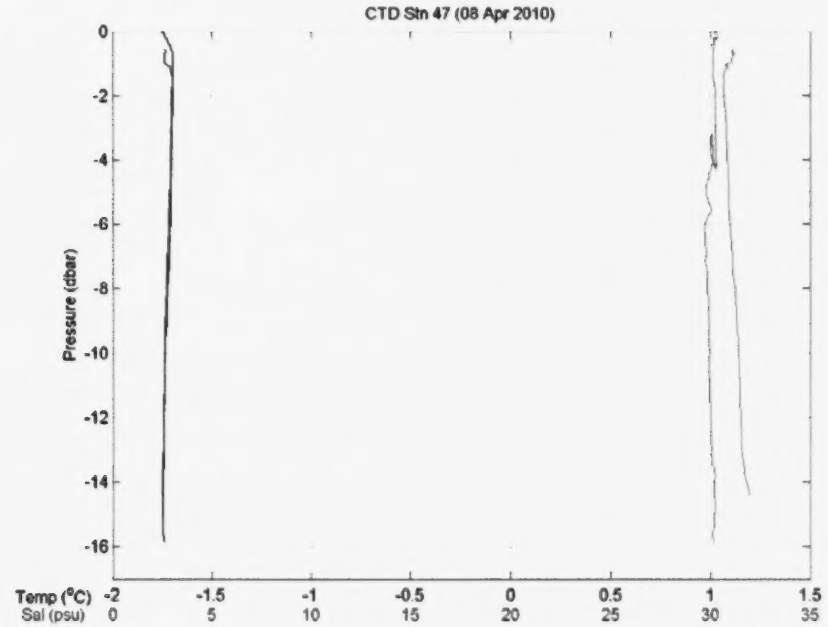

Fig. 24 Salinity-temperature profile of Stn. 47 from April 8, 2010.

Table 3: Mackenzie Delta 2010 on-ice station data (April 8, 2010).

	Stn. 43	Stn. 44	Stn. 45	Stn. 46	Stn. 47	Stn. 48
Latitude (° N)	69 32.58	69 34.20	69 36.60	69 41.76	69 48.00	69 34.41
Longitude (° W)	135 53.04	136 1.20	136 12.00	136 26.04	136 13.80	136 01.57
Time (MDT)	15:35	16:10	15:20	14:50	14:04	15:56
Snow thickness (m)	.29,.27, .30,.35	.08,.02, .01,.11	.15,.12,.12, .10,.08,.08	.05	.10,.08, .09	0.00
Ice thickness (m)	1.28	1.69	1.3,1.3	.90,.91	1.11	
Freeboard (m)	-0.005	0.17	0.08	--	0.11	
Water depth (m)	4.1	5.8	8.6	14.2	15.5	
Salinity (snow bottom)	14,14	12,12	15,15	18,18	16,16	
Salinity (0-5cm)	5,5	5,5	9,9	6,6	15,15	2,2
Salinity (50cm)	0,0	2,2	2,2	3,2,3	6,6	
Salinity (100cm)	2,2	0,0	2,2	2,2	14,14	
Salinity (water)	0	---	0	3	30	

The salinity samples within the ice at depths of 1-5cm, 50cm and 100cm at the inshore stations 43, 44 and 45 (Table 3), show that when the ice was formed in the late fall, the water column at those locations consisted of seawater, not the freshwater runoff that was present in April. The snow salinity content verifies this, and suggests that there was significant brine rejection during ice growth, or surface flooding of seawater due to snow loading (Table 3). At Stn. 43, the thick snow layer caused the negative freeboard and possibly reduced ice growth.

Combining EM-GPR-Video-Photographs

Small Lead

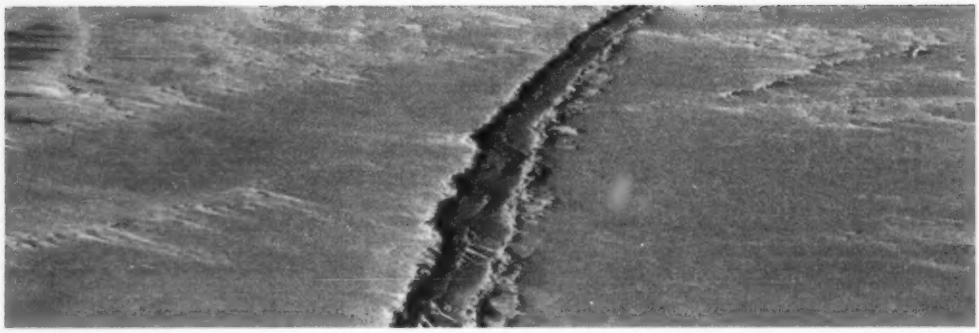

Fig. 25 Photo of small ridge/lead taken at 100m altitude between stations 16 and 17 on April 1.

In further analysis all data sources will be used: EM, GPR, Video, laser and photographs. Combining these data sources provides more details of the pack ice properties than that can be obtained from just looking at each source separately, i.e. the value of the combination is bigger than sum of its parts. Along the flight line between stations 16 and 17, a small lead was passed over that demarcated the land-fast from the mobile pack ice (Fig. 25). This lead was also shown above in Figs. 18 and 19 taken by the video camera. This small lead can be seen in the EM profile plot at sample number ~2.672×10^4 in Fig. 26.

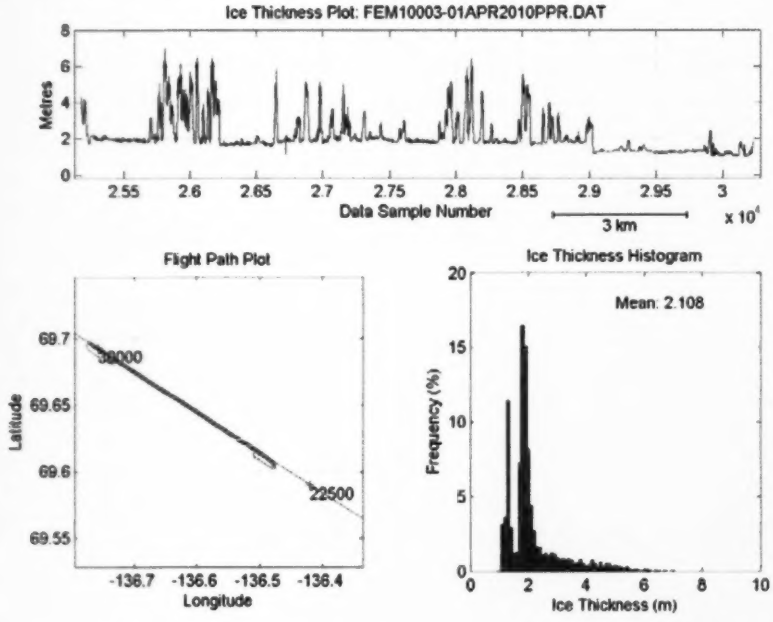

Fig. 26 The fifth of six EM sub-sections along the flight line between Stns. 15 and 17.

Fig. 27 shows an enlargement of ice thickness in the lead region, along with other parameters such as lower layer conductivity. In a plot of GPR data (Fig. 28), two closely spaced ridges on either side of the lead are visible, and appear to be ½ to ¾ m in height.

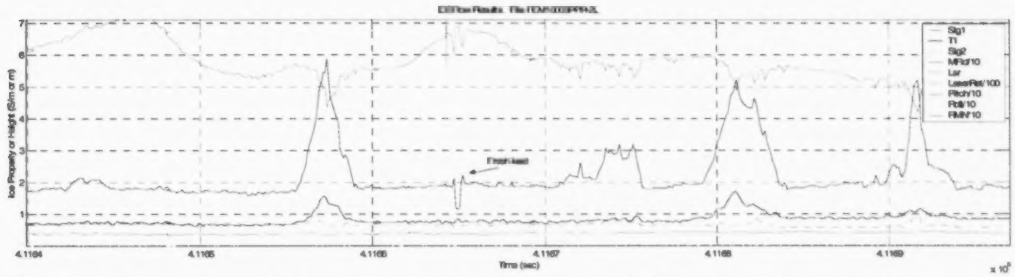

Fig. 27 Profile extracted from FEM10003; narrow lead shown as a decrease in ice thickness in the middle of the plot. Profile runs south to north and vertical gridlines are 10 seconds or approximately 300m apart.

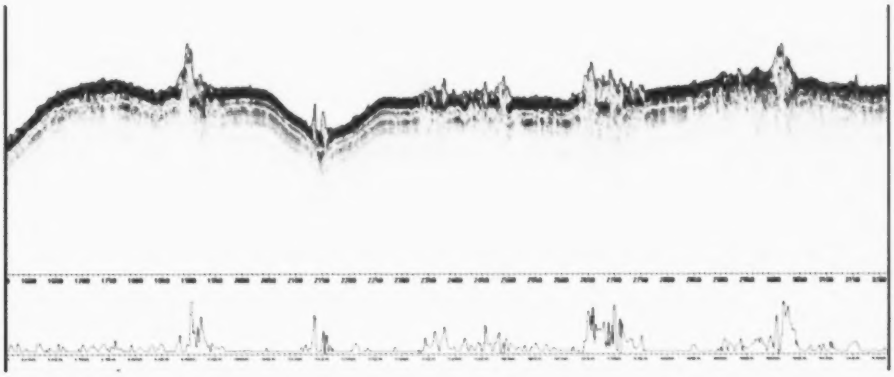

Fig. 28 GPR plot section for F560 where the small lead occurs, and is shown by two laser peaks at sample #2150.

The GPR plot (Fig. 28) was moved to the right to align its laser or ice roughness features with features of the EM plot (Fig. 27). Very little snow is visible on the pack ice on either side of the small lead. The other larger ridge peaks also align with the EM plot (Fig. 27). The bare ice can be seen in the photo (Fig. 25, left top corner).

Other figures for FEM10003 (April 1)

Figs. 29 and 30 below show the EM 5th and 6th sub-sections of the FEM10003 line between Stns. 15 and 17 using the post-processing plot routines. They show details of ice thickness (T1), laser (Lsr), and bottom layer conductivity (Sg2). Fig. 29 shows the 5th sub-section where the small lead shown above is present at ~4.11653sec. This data section was also shown in Fig. 26 by a different simpler quick-look EM plot routine used to E-mail the data to other users. The rough ice section (time section 4.1255 to 4.127x10x^{5}sec) is where the IOS mooring is located at Stn. 17 (Fig. 30); it was also shown by the simpler quick-look plot in Fig. 11.

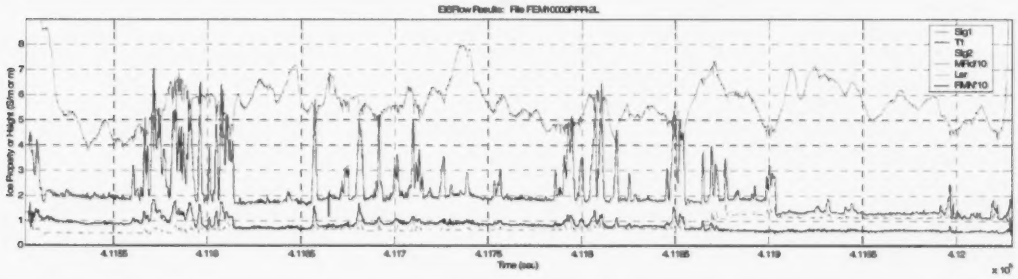

Fig. 29 FEM10003 Pic profile plot of sub-section 5 where the small lead was present and shown by the expanded plot in Fig. 27. Apparent water conductivity continues to rise, mainly beyond thick ridges that cause ponding of freshwater under ice.

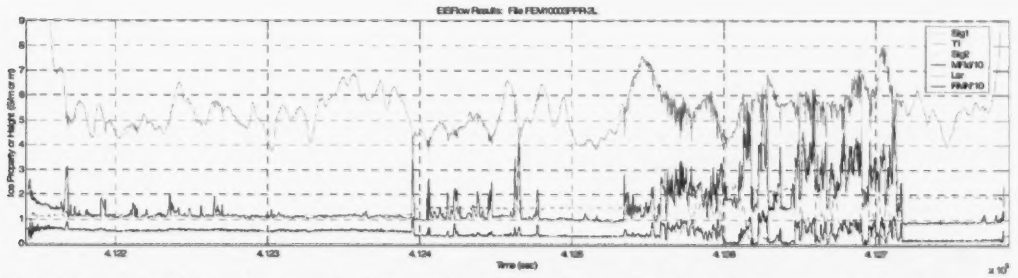

Fig. 30 FEM10003 Pic profile plot of the offshore sub-section 6. It covers the offshore mobile ice area where Stn. 17 (IOS mooring) was located beneath the rough rubble field and shown also in Fig. 11. Note multiple increases in apparent water conductivity, with the northernmost refrozen lead section just below 2 S/m.

Bottom-Fast Ice (BFI)

Waters off the Mackenzie Delta are shallow, with an area less than 2m deep extending for about 17 miles from shore (Stevens et al., 2008). Thus the ice, with expected ice thickness of 1.8m, is overlying either (a) seasonally frozen sediment over a permafrost layer (deep-frozen bottom-fast ice), (b) seasonally frozen sediment over unfrozen sediment (talik layer) over a permafrost layer (shallow-frozen bottom-fast ice), or (3) water over unfrozen sediment. The ice areas frozen to the bottom have a lower

elevation because they haven't been jacked upwards by fluctuating tide levels, so during freshet, runoff flows over the ice into the bottom-fast areas. Ice frozen to the bottom appears dark in SAR satellite imagery and does not give a clear reflective interface return for the helicopter-borne GPR. The EM on the other hand may be able to differentiate between shallow- and deep-frozen bottom-fast ice, since it returns "depth of the ice plus the frozen sediment layer". The GPR will give a clear return from the bottom of the ice if the brine volume is not too high. The information from EM and GPR thus complement each other and help to understand the complex ice properties of the shallow Delta region.

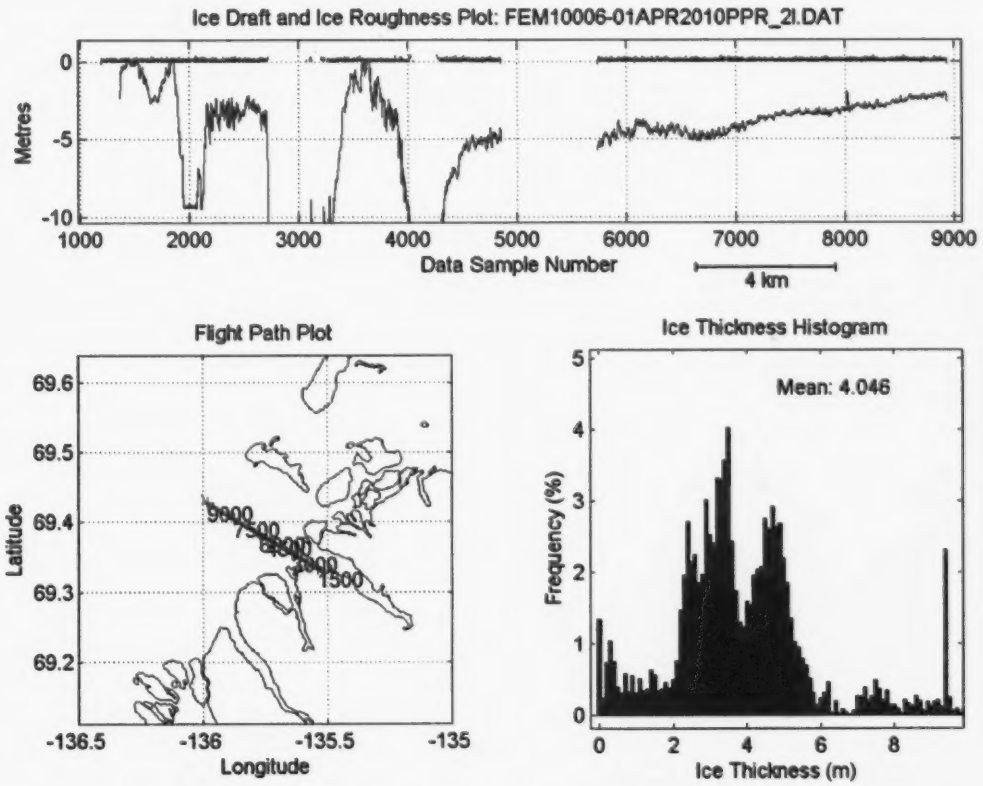

Fig. 31 Quick-look "ice thickness" profile plot for the total FEM10006 line of April 1.

The first example (Figs. 31 to 37) is from the line between Stns. 19 and 18 (FEM10006) where Steve Solomon of GSC-Atlantic is collecting on-ice data. Fig. 31 shows that the flight line between Stns. 19 and 18 consists of two sub-sections. For the inshore shallow sub-section, the EM upper layer thickness corresponds to the depth of ocean bottom, or identifies bottom-fast ice areas where thicknesses are greater than 10m. In the second offshore sub-section, the upper layer thickness first corresponds to the ocean bottom depth (around ~5m), then farther offshore, it corresponds to the depth of the freshwater plume and decreases in the offshore direction. A plot of the upper layer thickness and other variables for the inshore section is shown in Fig. 32 below.

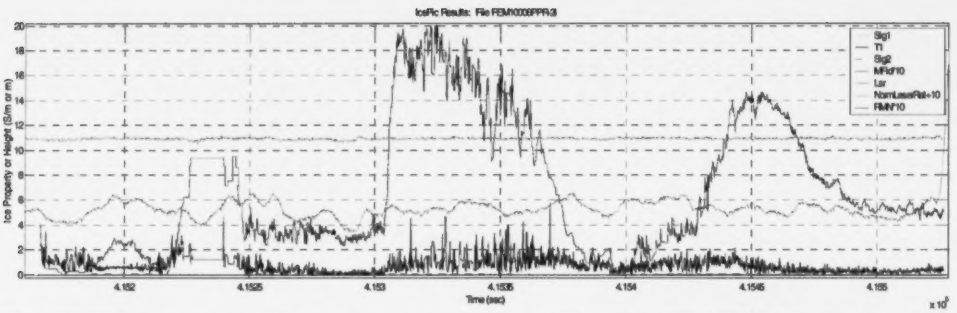

Fig. 32 EM upper layer thickness and other variables for FEM10006 inshore sub-section on April 1.

Figs. 31 and 32 show that the EM detects two major areas where the ice is bottom-fast, with thicknesses of 18m in the first area, and 14m decreasing to 5m in the second area. A third area also appears to be present inshore (left). The EM detects an upper layer thickness of 3m before the first major BFI region, and of 0-3m between the two major BFI regions.

The GPR acquisition over the same area (Fig. 33) started slightly later than Pic acquisition, hence the lateral shift of this image relative to Fig. 32 to align the features. The GPR data also show the two major BFI areas where the ice-bottom echo is weak, and the ice thickness is ~1m or less. For both areas, the zone of maximum EM upper layer thickness appears to correspond to the zone of minimum GPR ice thickness. The GPR data also show a ~1-1½ m thick ice layer before the first major area and between the two areas. To the north (right), the GPR plot shows a zone of frozen sediment overlain with less than 1m ice, while the EM data indicate an upper layer thickness (ice plus frozen sediment) of 5m. Again, the GPR and EM data are in agreement with the SAR data (Fig. 4), which show a dark-toned BFI area at the beginning of line F654, with two major BFI areas later in the profile.

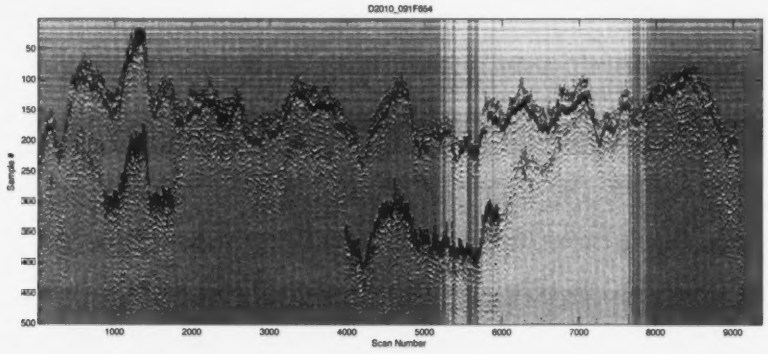

Fig. 33 Quick-look GPR plot a GPR section F654.

In the higher-quality GPR images below (Fig. 34) showing scan lines 1150 to 4750 of Fig.33, the edges of the first major BFI zone can clearly be seen. Note that there is a plotting gap between the left and right GPR images. To either side of the BFI feature, freshwater ice thicknesses of ~1-1½ m are present. The 1 GHz GPR does not

have enough penetration power to see if unfrozen sediment (talik) is present beneath the BFI. The EM data indicate an upper layer thickness (T1) of 3m before the BFI zone and 0-2m after the BFI zone. In contrast the EM data suggest large frozen sediment depths but provide no thickness for the overlying ice layer. The BFI zone in the EM and GPR plots correlates well at the edges, particularly the south (left) edge.

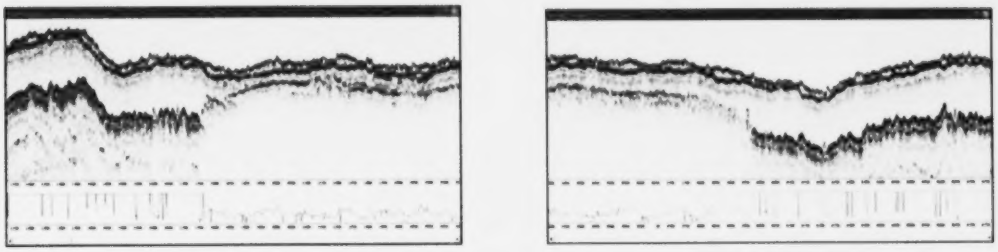

Fig. 34 GPR images for south and north edges of first major BFI feature in Fig. 32.

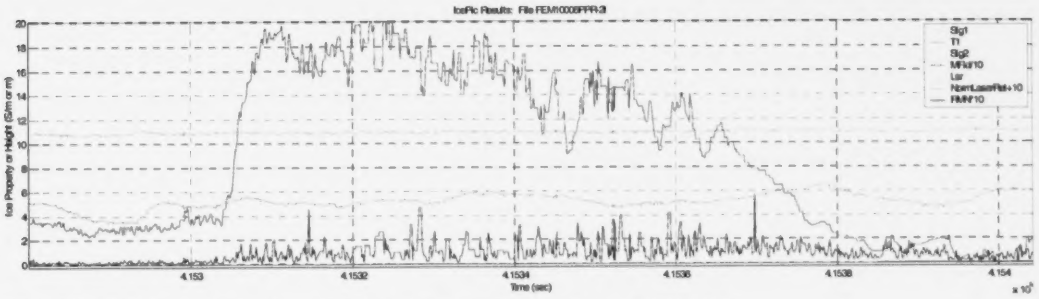

Fig. 35 EM data plot aligned with the two GPR plots of Fig. 34.

The second pair of EM (Fig. 37) and GPR (Fig. 36) plots show the second major BFI feature of the inshore line sub-section between stations 19 and 18 as seen in Figs. 31 and 32.

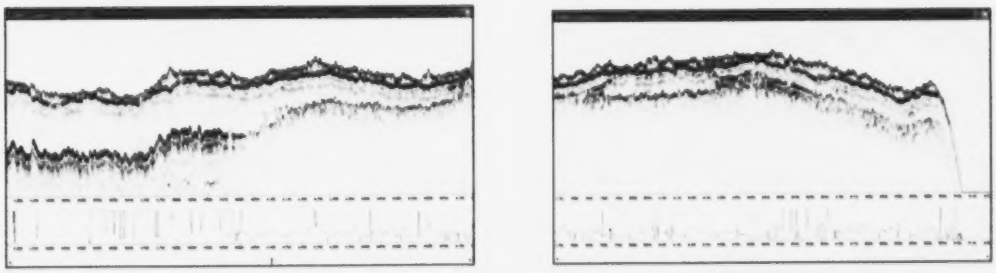

Fig. 36 GPR plots of the edges of the second major BFI feature shown in Fig. 33.

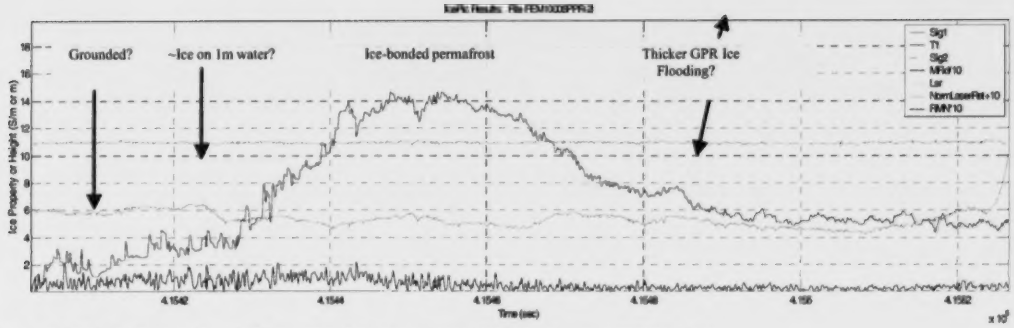

Fig. 37 EM data plot aligned with the two GPR plots of Fig. 36.

The BFI zone of the EM and GPR plots (Fig. 36 and 37) correlate well at the south edge (left). The T1 (blue) Pic profile "ice thickness" suggests that the ~1-1½ m ice (from GPR data) is lying on the bottom at south end of this profile, then has about 2m of frozen sediment between ice and unfrozen sediment. The GPR indicates thinning ice over frozen sediments (shallow bathymetry) to the northern end of the first GPR image, while the EM indicates the ice is bonded to the frozen sediment.

Inshore Gravel Bar

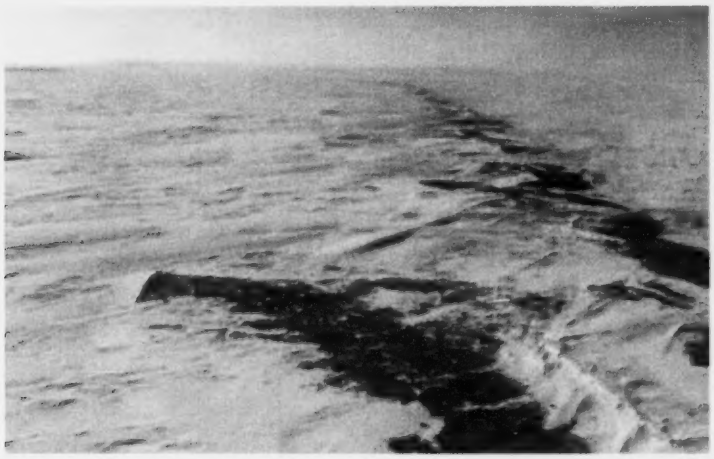

Fig. 38 Gravel bar seen inshore along the flight line between Stns. 5 and 2.

Along the flight line between Stns. 5 and 2 on April 1, a gravel bar was seen (Fig. 38). In the plot of the first section EM data (Fig. 39) along this line one sees a large BFI zone in the centre of the plot, in the general area of the gravel bar. Offshore the EM follows the ocean bottom topography to over 4m. The actual gravel bar is at sample #4350 as indicated by the small peak in the laser data (surface roughness) and it is the offshore edge of the large BFI zone.

GPR data for this area covering about 1500m are shown in Fig. 40, the gravel bar is located at sample #6800 where the laser peak is located. Snow depths of 30cm are clearly visible on both side of the gravel bar, as seen also in the picture of the gravel bar (Fig. 38). Inshore (left) of the gravel bar (laser peak), the weak ice-bottom echo indicates the ice appears to be less than 1m, and is bottom-fast as shown in the EM data (Fig. 39). Offshore (right) of the gravel bar, the GPR data indicates that at first, the ~1-1½ m thick ice is bottom-fast (weak reflections) but is then floating or resting on unfrozen sediment (stronger echo). At the gravel bar itself, there is little GPR reflection as the ice-frozen gravel is bonded to the permafrost and too deep to penetrate. Right at the peak, snow depths of 3/4m are present.

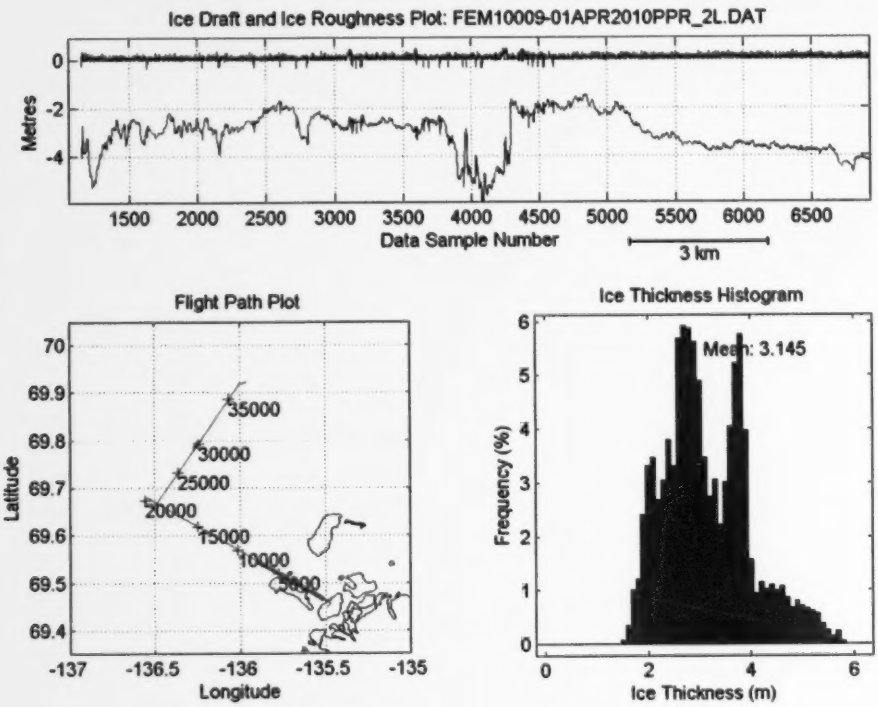

Fig. 39 First section of the EM data along the flight line between Stns. 5 and 2 of April 1.

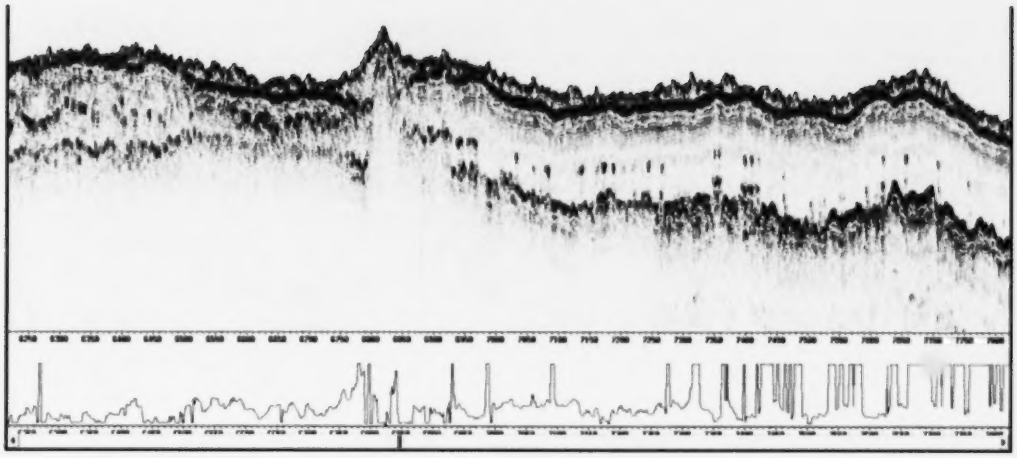

Fig. 40 GPR section plot covering ~1500m showing the gravel bar location.

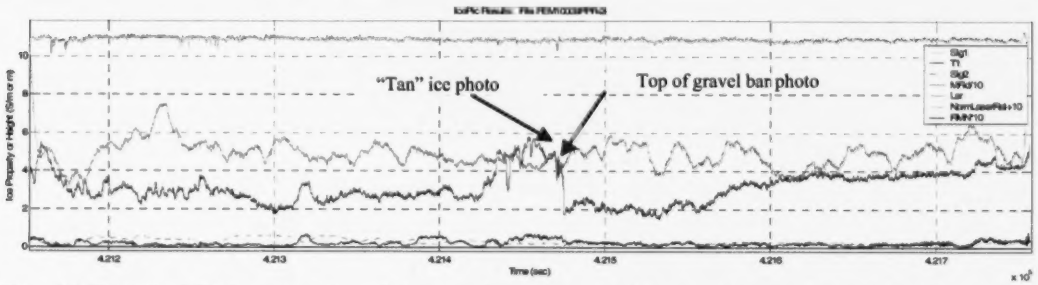

Fig. 41 Detailed EM parameter plot covering the gravel bar region and covering the same spatial area as shown in Fig. 39. The ice-bonded feature and gravel bar between fids 42140 and 42150 in plot above correspond to GPR scan range 5500 to 6500.

Fig. 42 Video frame 13240 showing the gravel bed collected on April1, 16:35. The video data were collected on the way back (south), so the top of the image is the inshore end.

Bare Ice Areas

Another interesting feature was a large area of bare ice immediately south of a large rough ice area, which is found north of the 5m contour. This was seen in several of the flights of April 1. The photograph shown in Fig. 43 shows this smooth bare ice toward the south, with the rough area in the foreground. The ice was probably kept bare of snow by northerly winds, which would allow snot to accumulate in the rough ice, but would blow snow over the bare ice downwind where it would accumulate. Snow could not adhere to the smooth surface and due to the lack of the snow insulation ice grow thicker than the surrounding snow covered areas.

Fig. 43 Photo taken along video flight from line 2 to 5 (April 1) looking south.

Fig. 44 Mosaic of the bare ice feature made from four overlapping frames of April 1 at 16:22, frame #12587.

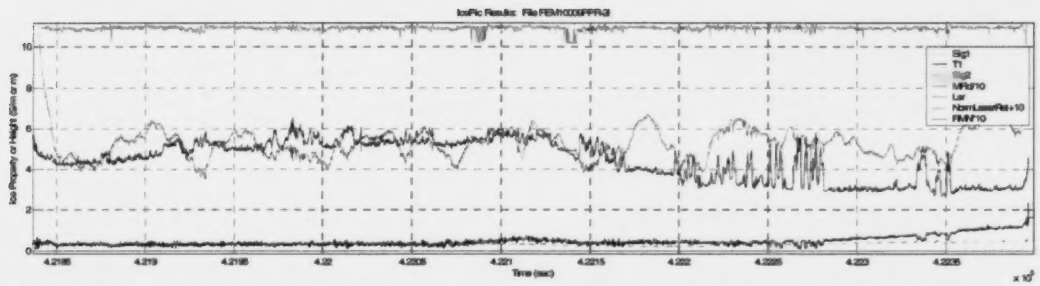

Fig. 45 Detailed EM parameter plot of second sub-section of FEM100009, line from Stn. 5 to Stns. 2 and 3.

A video mosaic of the bare ice region is shown in Fig. 44, with the rough ice area on the right. Figure 45 shows a plot of parameters derived from the EM system. Two areas with reduced laser brightness (green line) correspond to bare ice areas. The second bare ice region occurs just before (south of) an increase in ice roughness, shown by the upper layer thickness (blue line) at 4.2214×10^5sec, as shown in the video mosaic (Fig. 45). This rough area can be seen in the GPR (right plot of Fig. 46) where the ice-bottom echo disappears and rough ice topography is seen. Inshore (left) where the bare ice is found, the GPR shows an area where there is a strong ice-bottom echo and very little snow. The strong echo is probably due to low brine volume in the ice, resulting from a lack of snow and therefore cold surface temperature. However there appears to be some reflection at 20cm, which is probably the ringing of the GPR surface signal (note that the total ice thickness is ~1-1½ m). Farther inshore other bare ice regions were observed in the GPR data (Fig. 46, left plot), some showing a strong ice-bottom echo with ice thickness of ~1-1½ m. The EM quick-look ice thickness plot covering this region is shown in Fig. 47.

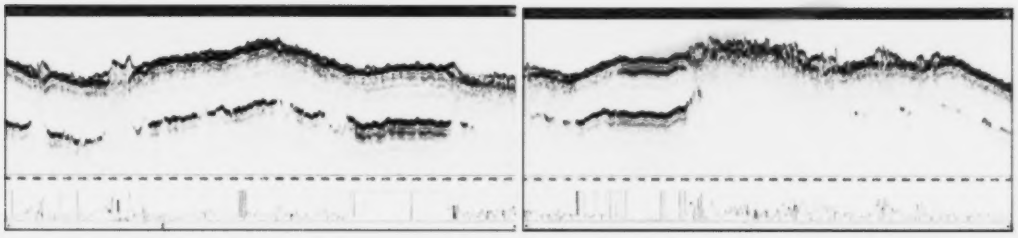

Fig. 46 GPR sub-section plots of file # 660 representing the second GPR section along the line between stations 5 and 2 on April 1.

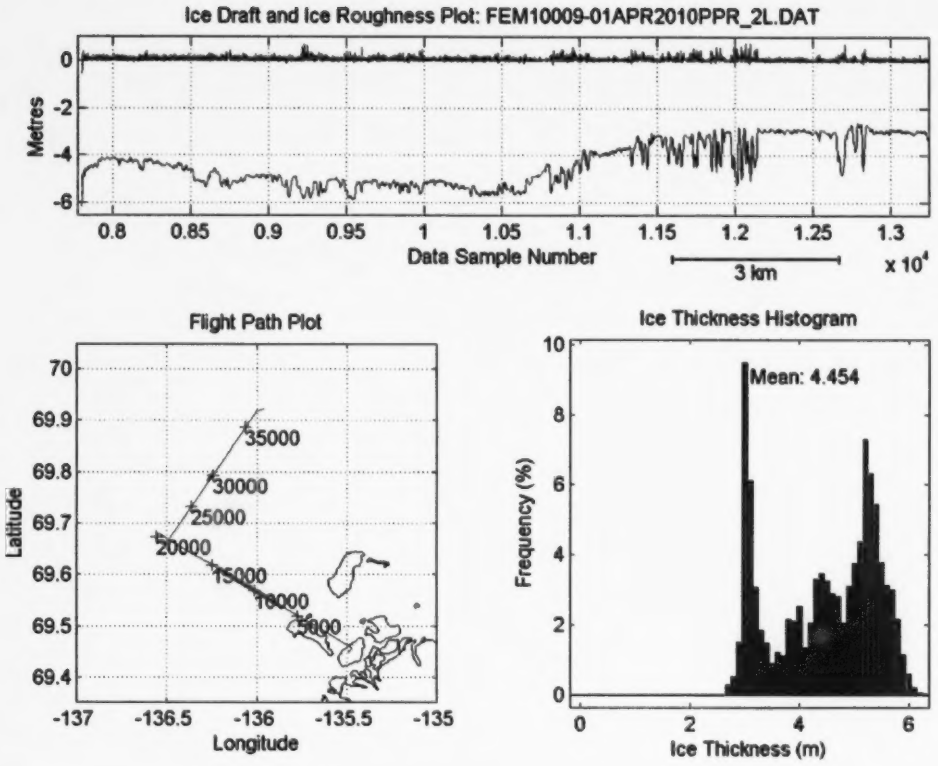

Fig. 47 EM quick plot showing the EM data along the same sub-section as for the GPR plot above, where the bare ice occurred south of the rough area that started at sample number 1.08×10^4 and shown in the right panel of Fig. 46. At this place the EM inferred upper layer thickness started to follow the bottom of the freshwater plume layer rather than the ocean bottom, and the GPR ice-bottom echo faded due to increased salinity of the ice cover.

Ridges and Leads

Fig. 48 Rough ice along the April 1 flight path and identified as the 3th EM sub-section FEM10009.

Along the last sub-section between Stns. 5 and 2 on April 1, a ridge with a large sail height (Fig. 48) was seen on the south side of a rubble field, with Stn. 2 located on the north side (Fig. 49). Data sample numbers are 1.78×10^4 for the ridge and 1.85×10^4 for Stn. 2. Beyond Stn. 2 for about 1km, the upper layer thickness is very homogeneous and just under 2m. The low conductivity of the lower layer (Fig. 50) indicates that the profile is within the freshwater plume area. This was verified by the CTD trace of station #46 shown in Fig. 23.

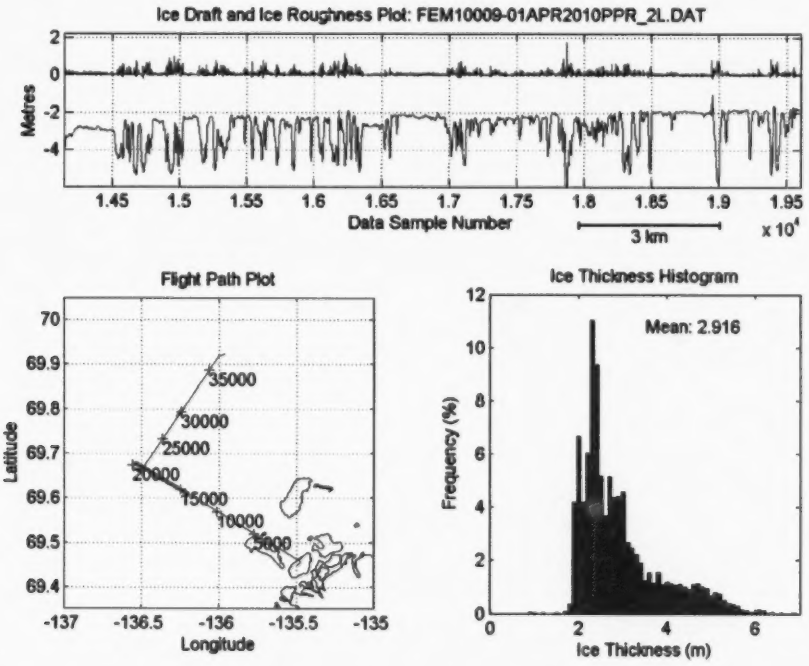

Fig. 49 Quick-look upper-layer thickness profile data of the 3th sub-section of FEM1009, April 1.

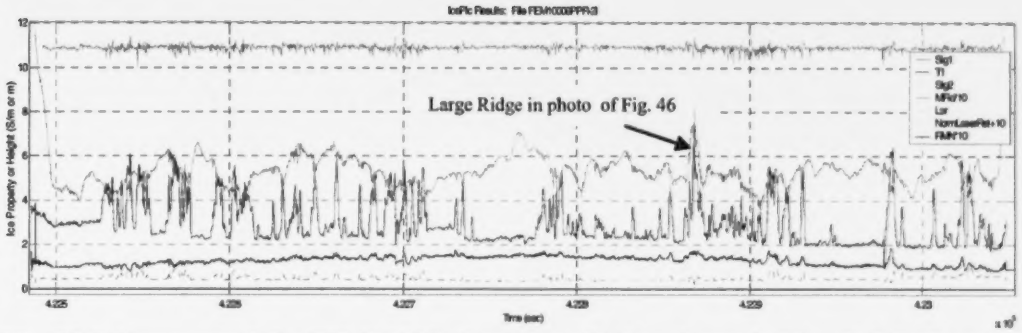

Fig. 50 Sub-segment 3 for FEM10009. Location of ridge shown in Fig. 47 is indicated in figure.

The small lead shown in Fig. 25 was passed over again several kilometres to the northeast near the end of the third sub-segment of FEM10009 (Fig. 51). The EM data and location of the lead are plotted in Fig. 51. The lead is shown in video file F034 at 16:13, frame #11658 (Fig. 52), and is perpendicular to the flight path and thus directed in SW to NE direction.

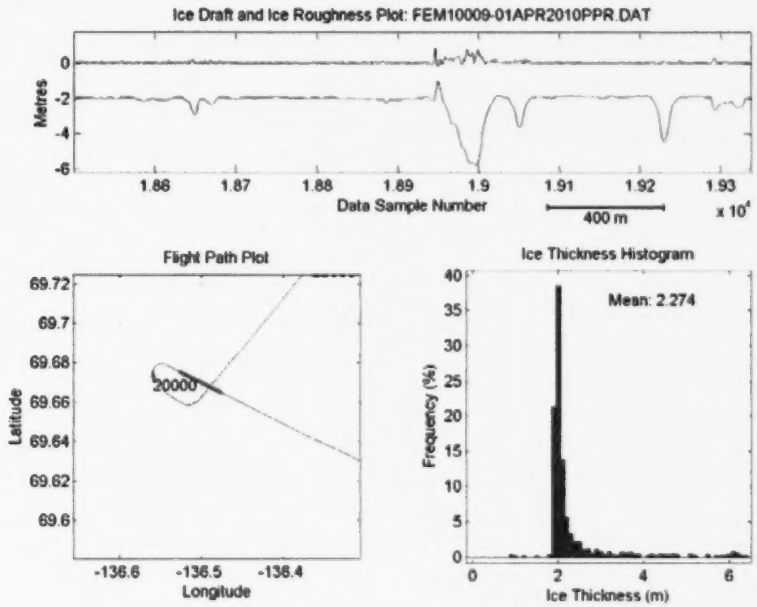

Fig. 51 Sub-section of the turning loop just past Stn. 2 showing the small lead with low ice thickness, just before a ridge feature.

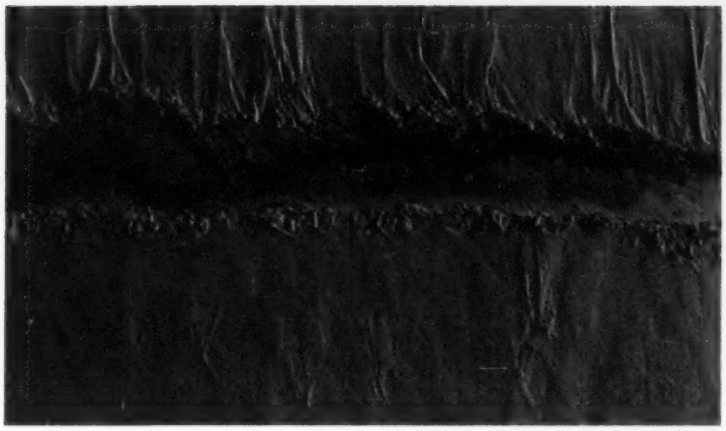

Fig. 52 Small lead northwest of Stn. 2, 16:13 April 1, frame F034-11658. With a video frame width of ~100m, the lead is about ~15m wide. The top is toward the northwest.

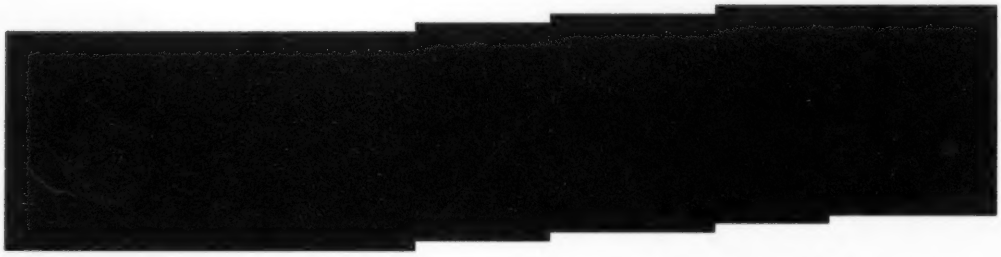

Fig. 53 Mosaic of small lead (Fig. 52) and ridge observed along the start of the line between Stn. 2 and Stn. 5, April 1, 16:13 Video file F034. The left is towards the northwest.

After turning at Stn. 2 toward Stn. 3 in the northeast, the ice cover (Fig. 54) appeared extremely deformed, with a couple of refrozen leads and very rough ice topography. The region is anchored in place by the rubble fields generated by artificial shoals such as the Minuk I-53 artificial island and the Tarsiut N-44 Caisson site. The old leads are characterized by homogeneous ice thicknesses, with values less than the modal ice thickness of ~1.5m (Fig. 54). The modal ice thickness of 1.5m probably represents the thermodynamic ice growth thickness of the area for this particular winter. Two refrozen leads can be seen; one with an ice thickness of 30cm at sample number 3.55×10^4, and one with an ice thickness of 80cm and ridges at sample number 3.4×10^4. The water conductivity is generally greater than 2 S/m for this profile (Fig. 55), much higher than for the profile on the inshore side of the deformed ice area (Fig. 50).

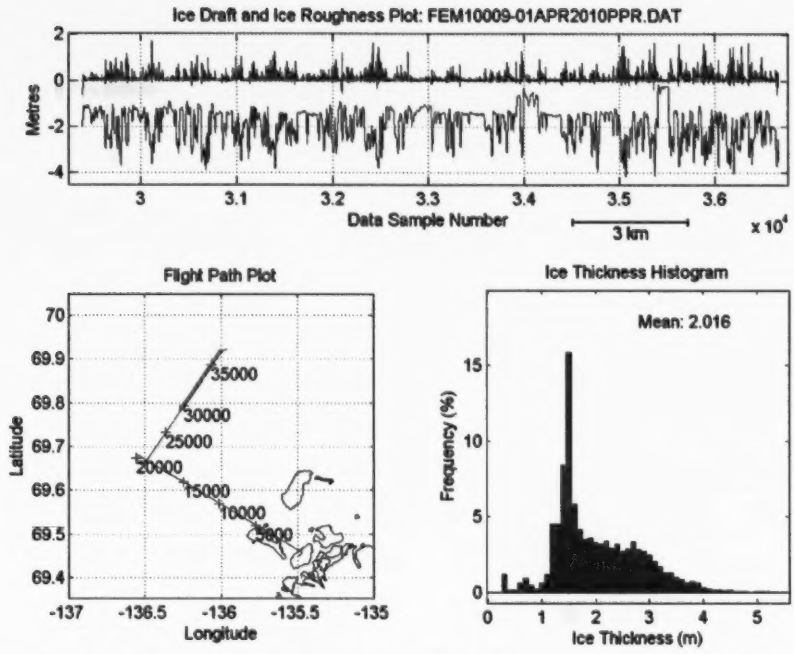

Fig. 54 Quick-look plot of upper-layer thickness for sub-section 5 of FEM10009 on April 1. The location where the profile thickness data was collected is shown by the green line.

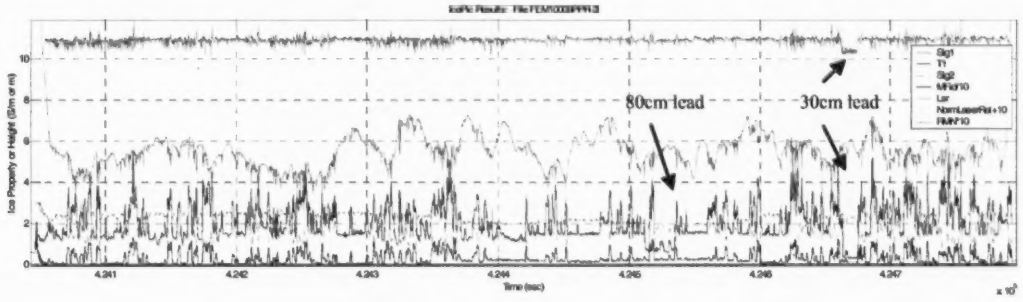

Fig. 55 Sub-section 5 of FEM10009. The water conductivity reached its maximum near the start of this segment and declined toward the eastern end. Note the 30cm refrozen lead near right side, with corresponding dip (upward-pointing arrow) in normalized laser intensity.

The surface of the lead with an ice thickness of 30cm had remnants of frost flowers and was relatively dark visually (left photo in Fig. 56). It also showed a decrease in normalized laser intensity (Fig. 55). The lead with an ice thickness of 80cm did not show a substantial decrease in brightness (right photo in Fig. 56) or laser intensity (Fig. 55). It had more snow on it and had been deformed (right photo Fig. 56). The photos were taken along the video flight back from Stn. 3 to Stn. 2. The thin-ice lead is shown as a single video frame in Fig. 57 and as a mosaic in Fig. 59. The thicker-ice lead (80cm) is shown as a single frame in Fig. 58 and as a mosaic in Fig. 60.

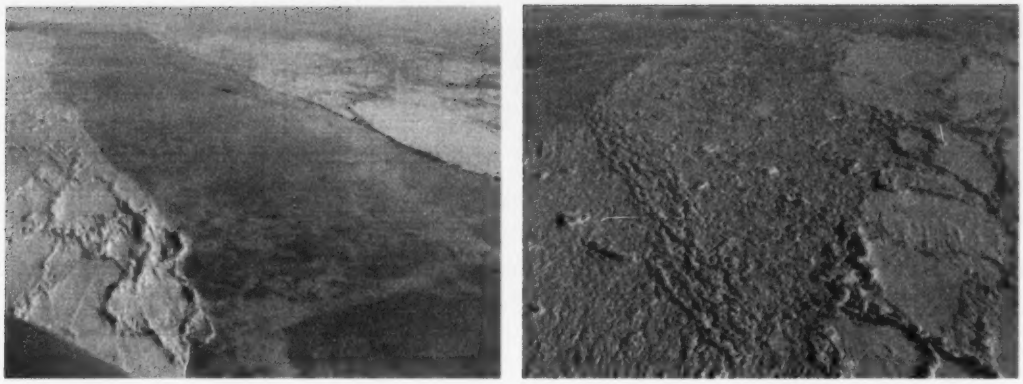

Fig. 56 Left photo is the lead with 30cm thick ice and low laser reflectivity; the right photo is of the lead with 80cm thick ice that shows higher laser reflectivity.

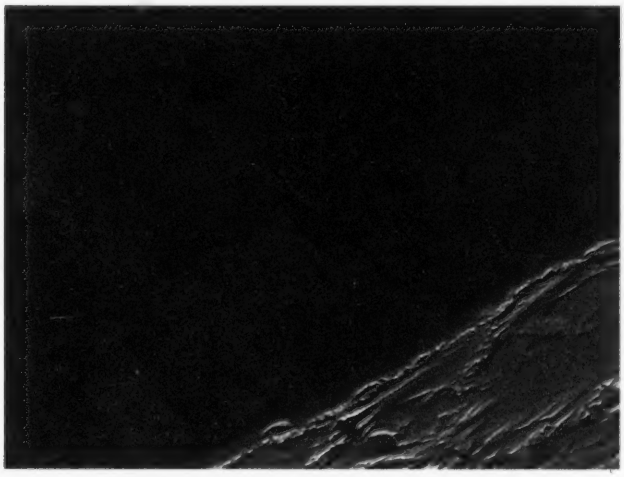

Fig. 57 Video frame #10527-F033 of April 1, 16:02 MDT showing edge of lead with ice thickness of 30cm.

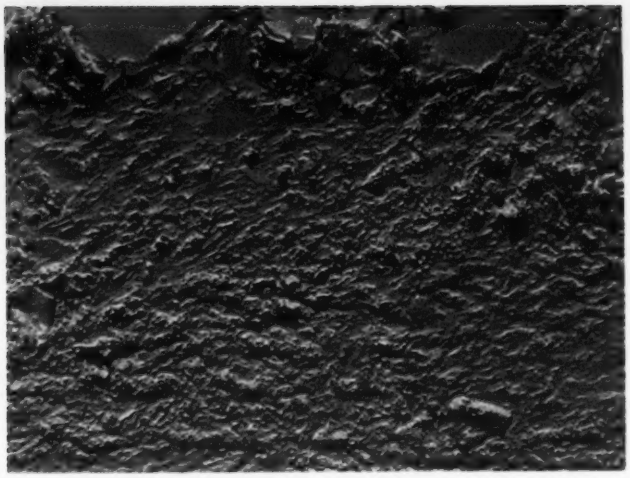

Fig. 58 Video frame #10568-F033 of April1, 16:02 MDT showing edge of lead with an ice thickness of 80cm.

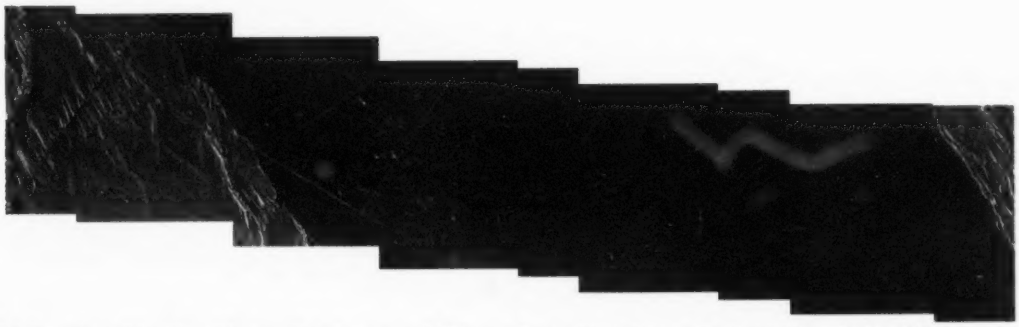

Fig. 59 Mosaic of lead with ice thickness of 30cm along line from St. 3 to Stn. 2 April 1, 16:02.

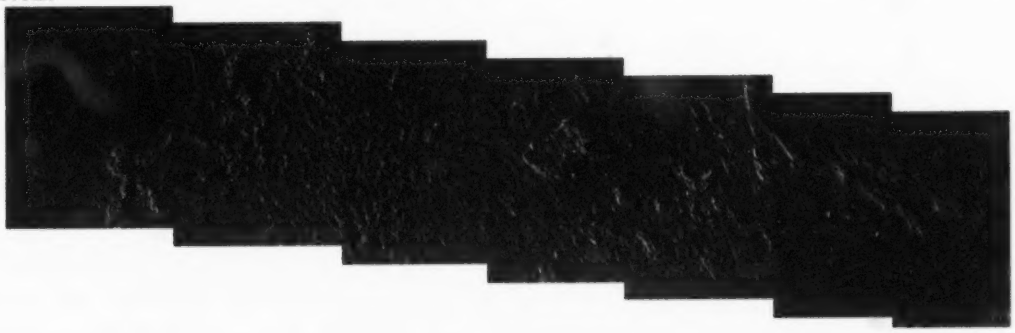

Fig. 60 Mosaic of lead with ice thickness of 80cm along line from Stn. 3 to Stn. 2 on April 1, 16:02.

Conclusion

This technical report described samples of data collected during the April 2010 sea ice survey off the Mackenzie Delta, NWT. No instrumentation delays were encountered during the 10-day survey, of which only 5 days or part of 5 days were used to collect data. During the remaining 5 days, the weather was unsuitable to work over the pack ice due to earlier than normal spring conditions. Data samples of the first day were highlighted in this report since those data were post-processed in the field during the weather delay periods.

The GPR, although new as a survey tool, worked continuously and will now provide another data set of ice and snow properties in additional to the Electromagnetic (EM), Laser and Video data sets. It complements the EM-Laser sensor data by providing snow depths, and low salinity ice thicknesses. In shallow inshore delta areas such as the Mackenzie Delta where river runoff dilutes the oceanic water, the GPR and EM together can differentiate floating or grounded ice from bottom-fast ice. The EM on its own can only provide the thickness of the snow-plus-ice-plus-frozen-sediment layer, however in these low salinity areas the GPR can also provide snow depth and ice thickness.

The laser brightness when normalized with respect to height, appears to be an additional observation tool to pinpoint young leads and dark features such as gravel bars. This technology will be expanded further to provide a better estimate of the open water versus ice fractions over-flown by the EM-laser and GPR-Laser systems.

All raw and processed data, plots, reports and papers will be available through the "SeaIce" website:http://www.mar.dfo-mpo.gc.ca/science/ocean/seaice/public.html and through the website's data link to the DFO Maritimes' FTP site: ftp://starfish.mar.dfo-mpo.gc.ca/pub/ocean/seaice/.

Acknowledgements

The authors would like to thank Canadian Helicopter Company personnel from Inuvik for their assistance during the survey. In particular CHC pilots Corey Arsenault and Jory Bott are thanked for their exceptionally smooth flying at low altitude, even during difficult weather conditions. James Pokiak of the Tuktoyaktuk Hunters and Trappers committee is thanked for obtaining permission for us to perform the survey without a wild-life observer on board; it was not known until we arrived in Inuvik that only instrumentation operators were allowed on board and only in the back seat during low-level survey flights. This work was supported by the Canadian Program of Energy Research Development (PERD), the Environmental Science and Research Fund (ESRF) and the Canadian Space Agency GRIP programs.

References

Fissel, D.B., J.R. Marko and M. M. de Saavedra Alvarez. The Changing Met-Ocean and Ice Conditions in the Beaufort Sea: Implications for Offshore Oil and Gas. Conf. proceedings, Int. Society of Offshore and Polar Engineering ISOPE-2009, Osaka, Japan, ISSN 1098-618: 636-642.

Kovacs, A., J.S. Holladay and C.J. Bergeron, 1995. The footprint/altitude ratio for helicopter electromagnetic sounding of sea-ice thickness: comparison of theoretical and field estimates. Geophysics, 60, 374-380.

Lalumiere, L. and S.J. Prinsenberg, 2009. Integration of a Helicopter-Based Ground Penetrating Radar (GPR) with a Laser, Video and GPS System. Conf. proceedings, Int. Society of Offshore and Polar Engineering ISOPE-2009, Osaka, Japan, ISSN 1098-618: 658-665.

Peterson, I.K., S.J. Prinsenberg and J.S. Holladay (2003). Sea-ice thickness measurement: Recent experiments using helicopter-borne electromagnetic systems. Recent Res. Devel. Geophysics, 5(2003): 1-20 ISBN:81-271-0026-9.

Peterson, I.K., S.J. Prinsenberg and Scott Holladay, 2008. Observation of Sea Ice Thickness, Surface Roughness and Ice Motion in Amundsen Gulf. *Journal of J. Geophys. Res., 113*, C06016, doi:10.1029/2007JC004456.

Prinsenberg, S.J., I.K. Peterson and Scott Holladay, 2008. Measuring the thicknesses of the freshwater-layer plume and sea ice in the land-fast ice region of the Mackenzie Delta using Helicopter-borne sensors. Journal of Marine Systems, Special Issue, Sea ice and life in a river-influenced Arctic shelf ecosystem, Eds. W.F. Vincent and C. Pedros-Alio, pp. 783-793.

Prinsenberg S.J., S Holladay and J. Lee, 2002 "Measuring ice thickness with EISFlow, a fixed mounted helicopter electromagnetic-laser system." Proceedings of the 12th Int. Offshore and Polar Eng. Conf. (ISOPE-2002) Kitakyushu, Japan, pp 737-741.

Richter-Menge, J, J. Overland, M. Svoboda, J. Box, M.J.J.E. Loonen, A. Proshutinsky, V. Romanovsky, D. Russell, C.D. Sawatzky, M. Simpkins, R. Armstrong, I. Ashik, L.-S. Bai, D. Bromwich, J. Cappelen, E. Carmack, J. Comiso, B. Ebbinge, I. Frolov, J.C. Gascard, M. Itoh, G.J. Jia, R. Krishfield, F. McLaughlin, W. Meier, N. Mikkelsen, J. Morison, T. Mote, S. Nghiem, D. Perovich, I. Polyakov, J.D. Reist, B. Rudels, U. Schauer, A. Shiklomanov, K . Shimada, V. Sokolov, M. Steele, M.-L. Timmermans, J. Toole, B. Veenhuis, D. Walker, J. Walsh, M. Wang, A. Weidick, C. Zöckler (2008). Arctic Report Card 2008, http://www.arctic.noaa.gov/reportcard/

Appendix 1: Station List

Stn #	Longitude	Latitude	Stn #	Longitude	Latitude
1	69 30.12	135 50.76	25	69 42.50	136 27.50
2	69 40.07	136 29.41	26	69 47.00	136 1.50
3	69 54.96	136 0.16	27	69 53.85	136 12.40
4	69 42.19	135 1.42	28	70 1.00	134 19.00
5	69 27.83	135 29.92	29	69 48.00	133 0.00
6	69 50.04	135 59.72	30	69 25.75	135 53.99
7	69 42.79	135 17.06	31	69 24.21	135 46.64
8	69 29.80	133 29.75	32	69 23.03	135 41.18
9	70 0.18	133 30.20	33	69 21.49	135 34.03
10	69 35.03	133 25.01	34	69 42.72	136 28.38
11	70 9.82	133 20.19	35	69 42.30	136 26.97
12	69 44.16	132 11.70	36	69 42.43	136 27.82
13	70 10.56	131 39.18	37	69 42.61	136 27.35
14	69 56.64	131 10.08	38	69 53.90	136 13.23
15	69 20.91	135 31.40	39	69 53.74	136 11.11
16	69 25.76	135 53.73	40	69 53.66	136 12.57
17	69 46.57	137 2.96	41	69 53.98	136 12.37
18	69 25.56	135 58.54	42	69 48.00	136 19.95
19	69 19.86	135 31.58	43	69 32.58	135 53.04
20	69 8.65	136 31.31	44	69 34.20	136 1.20
21	69 28.31	135 44.78	45	69 36.60	136 12.00
22	69 27.99	133 1.29	46	69 41.76	136 26.04
23	69 31.43	133 8.26	47	69 48.00	136 13.80
24	69 24.32	133 50.80	48	69 34.406	136 01.566

Appendix 2: Field Notes: Mackenzie Delta ice survey 2010

Wednesday March 31, 2010 overcast no winds -9°C

- Scott and Ingrid in Inuvik test fly the helicopter-borne systems and let the pilot Corey Arsenault get used to the system. No passengers are allowed in the front seat while surveying at low altitude.

- Simon flying from Calgary to Inuvik. Phoned James Pokiak about the problem that no wildlife observer can come along as a passenger. He will discuss it with the HTC.

- At CHC hanger in afternoon and met Corey. Change the Laptop back to PEI settings as the display screens were not active for the Video or GPR.

- Evening. Phoned James Pokiak and was told that they prefer an observer on board all the time, I told him they only can come while we do not use the instrumented helicopter for on ice work. He needs to talk this over with the THC. Phoned early again in the morning. Put new files on from disk send by Louis.

Thursday April 1, 2010 overcast, winds 290 at 10

- Phoned James Kokiak and they are giving us permission the fly, but on-ice work to go through Tuc: Wildlife observer and stops there. Ready to go by 10:00.

10:15 0n way to "Swimming Point" a fuel depot an hour north of Inuvik and closest fuel to the survey area. Scott and Simon in back of helicopter. The GPR new software does not work so replaced it back to PEI2010 settings. Left the Video settings as per new software from the Disc.

EM line out 15, 16 to 17. Clearing offshore and good contrast. I needed to change the computer time to Mountain Time which is 6hours behind UTC time: i.e. Computer is 11:26 MT, same as Camera and UTC time is 17:26.

GPR F644 west of Gradey Island very shallow and GPR sees bottom of ice and mud very strong ego. F645 at 17:48 and F46 at 17:55 with backgrounds for PIC in between. Ridge at ~69.499, second ridge at 69.514 at 18:05 UTC, this ridge is north of a field of bare ice appears to have formed by overflowing water (ice is clear). 11:05 on F647.
BG at 11:17 and on line at 11:18 F649, I had to restart GPR.
Past over a narrow open water lead 63.64 at 11:20, 8 miles to go to 17 by 11:27.
BG done by 11:29 on GPR F651 very flat ice for a long time 1.5m thick.
Very little snow on some sections of ice, rough towards the end where station 17 was.

Turned to do Video on way back from 17, file F027. Very flat ice north of 17 but rough around 17 and then flat ice again south of it. Active shear lead at 11:17 69.72. We are over flat ice but major rough rubble areas both the E and W of inbound video line.
10-15m lead crack at 11:52 Scott has a picture frame #6522 on Video. And a major ridge at 6760 frame # at 11:55 rough ridge to the East Scott has a picture. Ridge at frame # 7300 at ~ 13:00.
Flat ice and no snow south of ridge #7380; is this caused by flooding the ice or just flat, smooth ice the snow can not attached to.

At the 16 loop back to continue because we thought we were at 15.
16-15 lost first part now on Video F030. Back to the browner bare ice patches 8392 at 13:17.

Line 19-18; GPR-Noggin needed a restart. 13:20 at F654, needed to shut it down.
Half way a BG 13:27 and on GPR F655. The Video back to fuel depot file # F031 11:34; at fuel depot at 14:00 and ready to go again by 14:30.

14:30 Video out to shore line F032. End Video before starting the GPR. But had to restart power to GPR F657 and it is finally working. Past over an offshore bar 15:04; BG at 15:08 16 miles to go start/restart F660. Areas of no snow at 15:091 ~69.60. Ridge hump at 15:27.01, very rough after this with snow captured. Flat ice appears to have very little snow on it. Large rubble field with thin blocks (25cm). Needed to restart laptop? BG at 15:45 at about 2/3 down the line. Rough ice topography at start snow in between peaks.

16:00 Video back at 100m. 10424 point #3. Some stranded rubble to South but not Tarsiut. F034. At 11780 we just finished to lope at Stn. #2 to turn towards Stn.#5. The stranded rubble fields are connected by concave 10-15m open lead shearing a bit but not ridging. Concave meaning rubble fields are the headlands of the less mobile inshore pack ice. 16:23 over ridge with the flat bare ice to the south. Then, later crossing the sand bar and some lagoon south of it with brownish ice patches.

Friday April 2, 2010 overcast, light winds, snowing

8:30 - at hanger weather not good until later in the day.
- back to hotel and typed in field notes.
13:30 - phoned hanger for update of weather, weather down, no surveying.
- Worked on GPR data and stored GPR data, no map plots of Images nor GPR although GPS data is there. Ingrid put all GPR data on Ftp website. Phoned (20:00) Tuc THC put message about re-delay survey on answering machine.

Saturday April 3, 2010 overcast, light winds, snowing

8:15 - phoned Tuc THC and left another message
8:30 - at hanger weather again not good until later in the day.
- back to hotel and worked on data to make sure GPR data is there for Steve Solomon lines.
13:30 - Corey phoned from the hanger for update of weather, weather down, no surveying. Ingrid working on video viewer to see if we can make it work fro GPR and video maps. Not all webpage files come through (too large files error message)
- Worked on GPR and EM data files.
Phoned Tuc THC put message re-delay survey on answering machine.

Sunday April 4, 2010 overcast, light winds, snowing

8:15 - phoned Tuc THC and left another message

8:30 - phoned hanger, wait till noon for weather report.
- At hotel and worked on data to screen grab GPR plots.

13:30 - Corey phoned from the hanger to say that the low of Tuc is hanging around and should cancel surveying for the day. Ingrid working on video viewer to plot GPR and video maps and corrected webpage error. Phoned Tuc THC put message re delay survey on answering machine.

Monday April 5, 2010 Clear, light winds, -12°C

8:15 - Hanger, weather improving throughout the day.

8:30 - At hanger and leaving by 09:20 for Swimming Point (10:20).

10:40 cloud bands overland and 4minutes out of Stn. 5.
Planning to do 5-26-27 EM-GPR out. Started but by 10:43 stop/start as no data showed up on plot 668 maybe empty now on GPR 669.

10:51 BG at the sand bar (63.5666), 10:52 over ridge, redid BG after I saw no laser again, fresh ridge just south of it, now on GPR #671. Major rubble field at 63.62447 at 10:59.20 after that very flat ice.

11:01 Rubble to east at 69.658. Small rubble are, white block, lots of snow in between. BG at end of rubble field with ¼ m thick blocks. Stop/restart again – only laser. Now recording GPR 673 at 11:08. Losing bottom of ice in data plot (11:09). Rough ice block thicker 1/2m and mostly blue. Rubble all the way to 11:13 (lots of pictures). Not ridges just all rubble. Major ridge at Stn. #26 (11:14); broke up line; then BG at 11:16, large 1-2m blocks. Needed to unplug GPR after lost BG; now logging GPR #677, not sure what #676 shows.

11:23 now in mobile ice going to Stn. #27. Lots of new thin leads, at #27 11:24, very thin ice at 10:26.0, changing to Video.

Going back to #27 and recording Video.

At Tarsuit flying lines W to E similar as and parallel to #38-#39.

1. Centre C line 38-39 and back to 38 by counter clockwise loop.
2. N+1 a line north and parallel of 38-39 by 150m
3. N+2, then 4. South and parallel to 38-39 (S+1), the a line W-E on return loop, the line S+2.

Placing lines half way in the between: N+1.5; N+.5, S+.5 and S1.5.

Fished and passing over from #27 to #25 and on to #5 and fuel.

12:08 At #25, rubble field 69.7668 and north to 69.7550.
Frame 16680 a lead at 12:10, at 12:16 row of rubble humps lining up as a E-W ridge, frame 17270. Inshore a small lead at 17557 (12:18.41) but distinct in flat ice. North of this all boring ice. This lead goes to tip of headlands. At Stn. #5 18051, on to fuel depot (12:45).

13:10 of to 5, 42 and 25 grid work. Weather better but still overcast.

13:31 GPR switch on/off over land.

Started at 13:34 GPR679, but turned it on/off as the plot showed no data. Restarted GPR #680 and it showed data, lots of snow (40cm +) as shown by GPR plot. Two pictures at 13:36, very boring ice, stop/start GPR again just laser (13:49).

Passing over a series of parallel-to-the-shore ridges.
At, 13:49.50, second at 13:51.00, third at 13:51.29 and fourth at 15:53.27. Lots of snow between these ridges. At 13:54.30 flat pack ice occurred; 3 pictures at 13:55. Then BG at 13:55. Trouble with GPR again, restarted it at last BG 14:07 now GPR 686.
14:09 major ridge area with .5m blocks, the rubble field, 5 pictures with lots of snow between rubble peaks, blue blocks with dirty brown bottoms.
Thinner blocks in flat ice area. Then flat ice area

BG at 14:12 now GPR 687, over flat ice, major ridge 3943 count rate on GPR, flat areas at 14:19.

BG at 14:21. At 14:24 blocks have brown algae bottoms, now on GPR #688.
Major rubble field, over lead at 14:27.0. Another end BG at 14:30 and Video back to #42 (F054).
Tried to start GPR but gave up too short a time before being at #25.

Rubble field grid lines: Points do not line up over the rubble so the line will be running at 100 degree from round end to narrow east end of the rubble field. W-E as centre line #59, return again as anti-clockwise loop. Return loop E-W id file 60. Then N+1 (61), then N+2 (62), N+3 (63). The south of centre line: S+1 (64) and S+2 (65) 15:03.

Going back to 25-42-5: From 25 to 42 saw small parallel leads at 45 to our track coming from #25 and still present when going from 42 to 5, but now at 90degrees. Back at Fuel depot at 3:55.

Off from depot at 4:25 test GPR #689 no plot again, stop/start and now on 3690. Maybe I am asking it too early?
At Stn. 16 stop and do BG then to go to Stn. 21, frozen patches of ice within the snow. At Stn. 21 16:58 #693 but plot blank so restarted it now #694.
At 15:02 crossed line 12-16 and later 19-18; the BG at 17:07.
Another BG at 17:21 some pictures, ice piles to North of line. Some pictures during BG. Ice very boring no rubble features. At end line more grounded ice features:
To left at 17:28.14, to far right at 17:31.67, and to left at 17:31.37
BG at #20 then turn to Tuktoyaktuk and did some Video at 250m F069 and F070 end at 17:42 and at hanger 18:30.
Phoned James but busy in bar with friends call back in morning.

Tuesday April 6, 2010 overcast, light winds, snowing

8:30 - phoned hanger, wait till noon for weather report.
- At hotel and worked on data inputs and plots.
13:30 - Went to hanger and split gear up for both on-ice work and survey work. Finished GPR plots.
14:30 - Left because of health Minister's visit, cancelled for the day. But clearing in Inuvik but overcast in Tuktoyaktuk.

Wednesday April 7, 2010 overcast, light winds, snowing

8:30 - phoned hanger, wait till noon for weather report.
- At hotel and worked on data, bought shovel and went to rental car agent. Start plotting PIC line plots.

13:30 - At hanger; weather not clearing, freezing layer aloft; left for hotel for more data processing.

Thursday April 8, 2010 overcast, light winds, snowing

8:30 - phoned hanger, wait till 11 for weather report.
- At hotel and worked on data, pre-paired for on-ice work

12:00 – after lunch went to hanger and packed two helicopters for afternoon work. On ice work along 5-2-3 line and EM-GPR to Tuktoyaktuk line.

13:00 - A-star left with Scott and Ingrid and 13:30 206-L left with SP.

14:43 - 206L via Swimming point for fuel. GPR test #698. Did line 24-23 Steve's inshore Tuktoyaktuk line (GPR 699-700), then PIC-GPR to #29 where a race track path was flown for both Pic and Video. PIC 2020.

15:24 - to 29 GPR 701 and GPR 702, ridge at ½ mile after BG. Another BG at 15:30 GPR 702 middle to stn 29. Large rubble field 1km to east 15:32; dirty bottom ice blocks of 1/4m thick (old).15:36 Rubble pile to east but closer ½ mile. Between 15:33 and 16:00 at Stn. 29 (GPR 703-704).

16:06 - Video at stn29 and back to Stn. 23 (F071- 75); PIC 1020 in and out; then fuel at Tuktoyaktuk.

17:10 -Tuktoyaktuk line 10-11; PIC-GPR out and Video back. PIC 2021.
Pic started right away and GPR needed two restarts, file 709.
BG at 17:17 GPR 709. Flat ice ends at 17:21.Change from flat to rough ice at17:23 no change in PIC conductivity. Rubble field at 17:26, many ridges at 17:31, then sections of flat ice at 17:32.
BG at change to GPR 711, at 17:31 possible a linear shear zone.
BG and now 712 at 17:41 rough ice started. BG and 713. Video (F076-78) back and on to Swimming point 18:51. Turned back to Tuktoyaktuk and on to Swimming point and Inuvik.

20:00 - Just made supper before restaurant closed. Changed tickets for flight home, to do video and back gear up.

Friday April 9, 2010 overcast, but clearing

8:30 - phoned hanger, wait till (9:30) for weather to improve.
- At hotel packing for trip home (Ingrid and Scott).

10:00 - left for Swimming point (two pilots). Ingrid and Scott packing some gear and labeling the boxes. 11:15 left depot to Stns. 5-25-27-5 triangle. PIC-GPR out to 25. 11:37 GPR 715, BG at 11:45 (716) and BG at 11:55 (717) short GPR 718 to 12:06.

10:10 GPR off and Video on.

Centre line over #25 F079, then S+1 Video F080, S+2 F081 and S+3 F082. The NE of centre line N+1 to N+4 for F083 to F086, Video F087 to Stn 27. Bear viewing somewhere just before Stn. 27.

12:59 - Video lines 0ver #27: centre line F088 done by 12:39, the S+1 tp S+3 for F089- F091. Long approach on N+1 F092 done at 12:49, then N+2 and N+3 for F092, F093 and F094.

13:00 - Start PIC-GPR over 27 and going to #5. Several BGs but last suction lost the GPR and could not start it. GPR up to 720, rest empty. It started over land (#724) after a complete shut down; so GPR okay but as real problem at times.

16:30 - All gear packed, just need to put in laptop in the morning and close the two boxes.

Appendix 3: GPR post processing

By: Louis Lalumiere, Sensors by Design, Ltd

Summary

The GPR profiles have the following:

- Sea ice only – no snow, very thin snow or a few drifts
- Snow over sea ice
- Snow over freshwater ice

Interestingly though, additional features are seen:

- Freshwater ice over a salty conductive media or sea ice (snow is also present)
- Rafted freshwater ice
- Subtle clues to variations in the brackish content of freshwater ice

The thickness results are calculated using an assumed dielectric constant of 1.5 for dry snow and 3.2 for freshwater ice.

GPR Profile plot Summary Tables

GPR Profile	Snow/Ice Condition Estimate	Comments
644	Thin snow layer Sea ice	Beginning and end of profile are transitions to/from fresh water ice under the snow. The weak echo from the bottom of the freshwater ice indicates that a saline conductive layer or sea ice is likely under the fresh water ice.
650	Thin snow and snow drifts Sea ice	Very thin snow with a few snow drifts up to approximately 30 cm (shown in report as Fig. 17)
655	Snow layer Freshwater ice	Freshwater ice in first half of profile has lots of what could be rafted ice near the bottom
656	Snow layer Freshwater ice	Echo strength of freshwater ice layer varies. The last half of the profile has a very strong echo and a multiple reflection from within the ice layer. Freshwater layer thickness starts at approx. 0.5 m and increases to approx. 1 m over the first 2 km of the 10km profile.

Snow Over Sea Ice - GPR Profiles: 644, 650

Since this data has mostly sea ice, the one-dimensional snow thickness processing was performed.

GPR Profile 644

Most of the profile has snow over bottom-fast ice. Floating thick freshwater ice (up to approximately 1.25 m) is seen at the beginning. Bottom-fast ice is seen clearly at the end.

There is a solid echo to follow for the bottom of the freshwater ice. At the beginning of the profile the thick freshwater ice tapers down from 1.25 m to near zero (where it is bottom-fast) over approx. 200 metres.

The echo from the bottom of the freshwater ice layer is weaker than the snow/ice echo. This leads one to believe that the ice is resting on unfrozen sediment as the echo from freshwater ice over water is normally stronger than the air/snow interface echo or the snow/ice interface echo. Plots provided at the end of this Appendix #3 – with snow thickness processing:

- Complete profile plot
- 4 plots to show profile at a larger scale

GPR Profile 650

This profile has very thin snow and a few snow drifts over sea ice.

Typical results from the past have shown that the snow thickness processing results show a zero value when no snow is present, as the first echo returned (the echo assumed for the snow surface) is also the strongest (the echo assumed for the snow/ice interface). When snow is present the strongest echo is no longer the first echo. With very thin layers the air/snow echo and the snow/ice echoes add together causing the largest peak/trough amplitude to vary.

The Noggin 1000 has an approximate pulse length of 1.5 ns. With the typical pulse consisting of a trough, a peak and a trough (or a peak, trough and a peak), the peak to trough distance is 0.5 ns. The snow thickness for a two-way travel time of 0.5 ns using a dielectric constant of 1.5 is approximately 0.06 m.

The snow thickness plot appears to show a bias of about 0.06 to 0.07 m for snow thickness, with some results of zero metres. This indicates that the GPR pulse's peaks and troughs limit the minimum resolvable snow thickness when snow is present to approximately 0.06 m.

Snow and Freshwater Ice Thickness – GPR Profile 655

The second half of profile 655 has very strong and consistent echoes for the air/snow, snow/ice and ice/water interfaces. Two-layer thickness processing was applied and the results are shown at end of this appendix and in the main text as Fig. 17.

GPR Profile with Bottom-fast Ice

A section of Profile 656 with a lot of features has been annotated (shown below) with a possible interpretation of the ice and snow conditions. The snow layer is approximately 35 cm thick in the deepest areas. The left-most freshwater ice layer is approximately 50 cm thick. The middle freshwater ice layer is approximately 1.2 m thick. The right-most freshwater layer is approximately 1.8 m thick. The along track distance between each GPR scan is approximately 1 m.

Multiple reflections can be detected by observing that the slope of the multiple is twice the slope of the first echo. In the region above the arrow pointing to the "multiple" reflection the ice

thickness gets slightly thinner and then thickens out again. The slope of the "multiple" echo shows the thickness changing at twice the rate of the ice thickness.

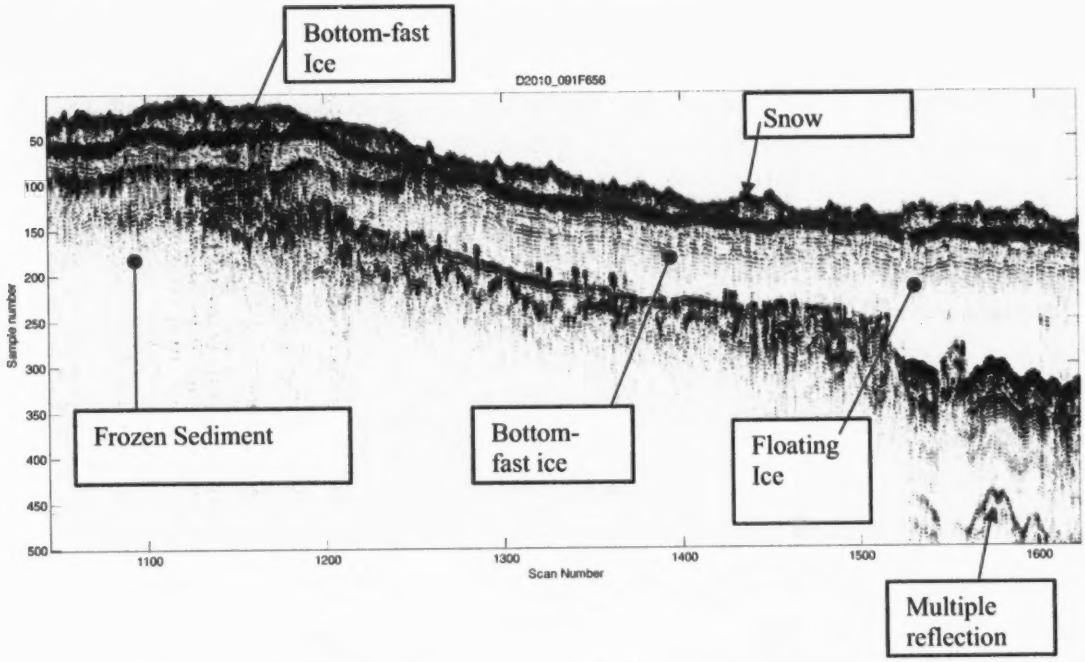

GPR profile 656 annotated with a possible interpretation of the snow and ice conditions.

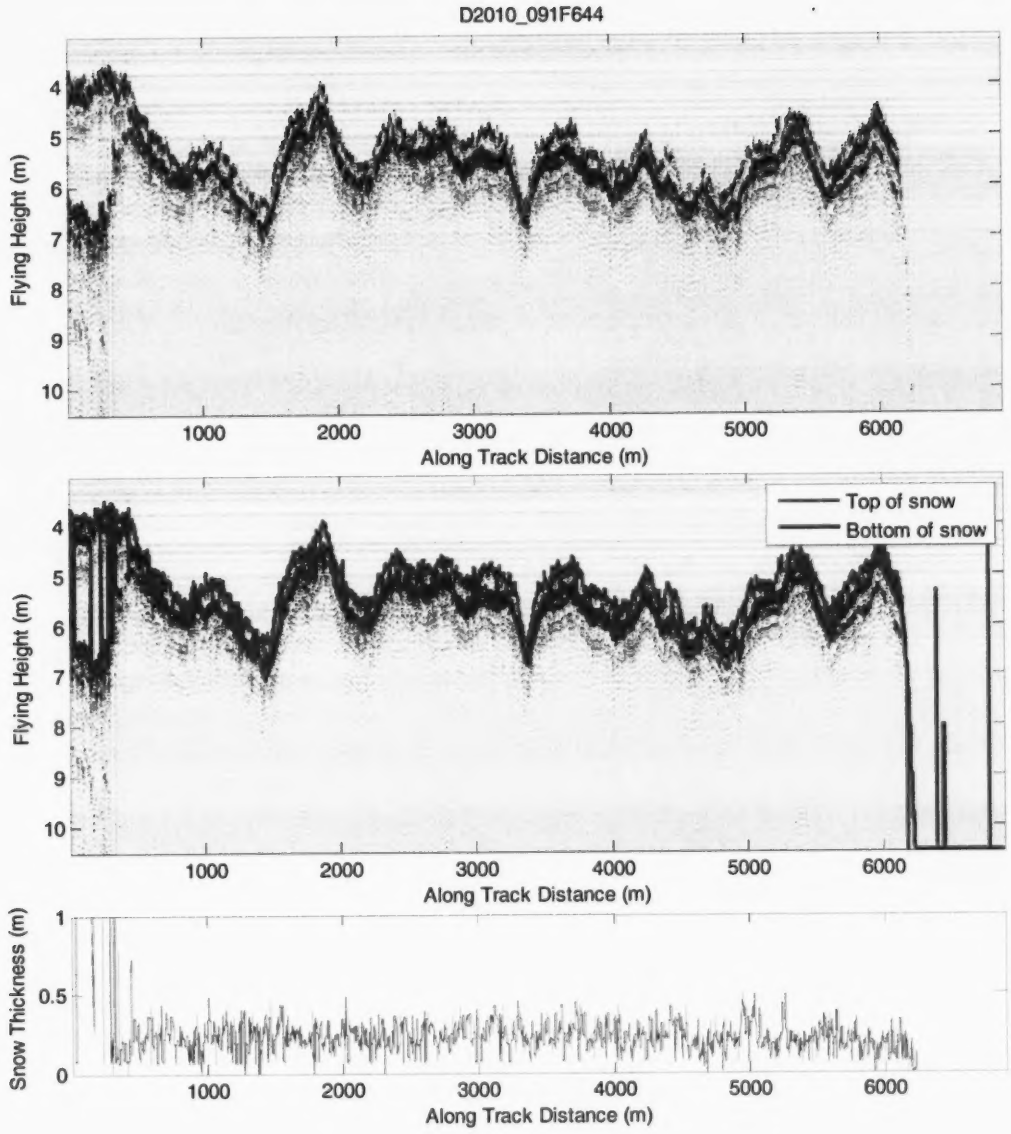

Plot of the complete GPR profile 644

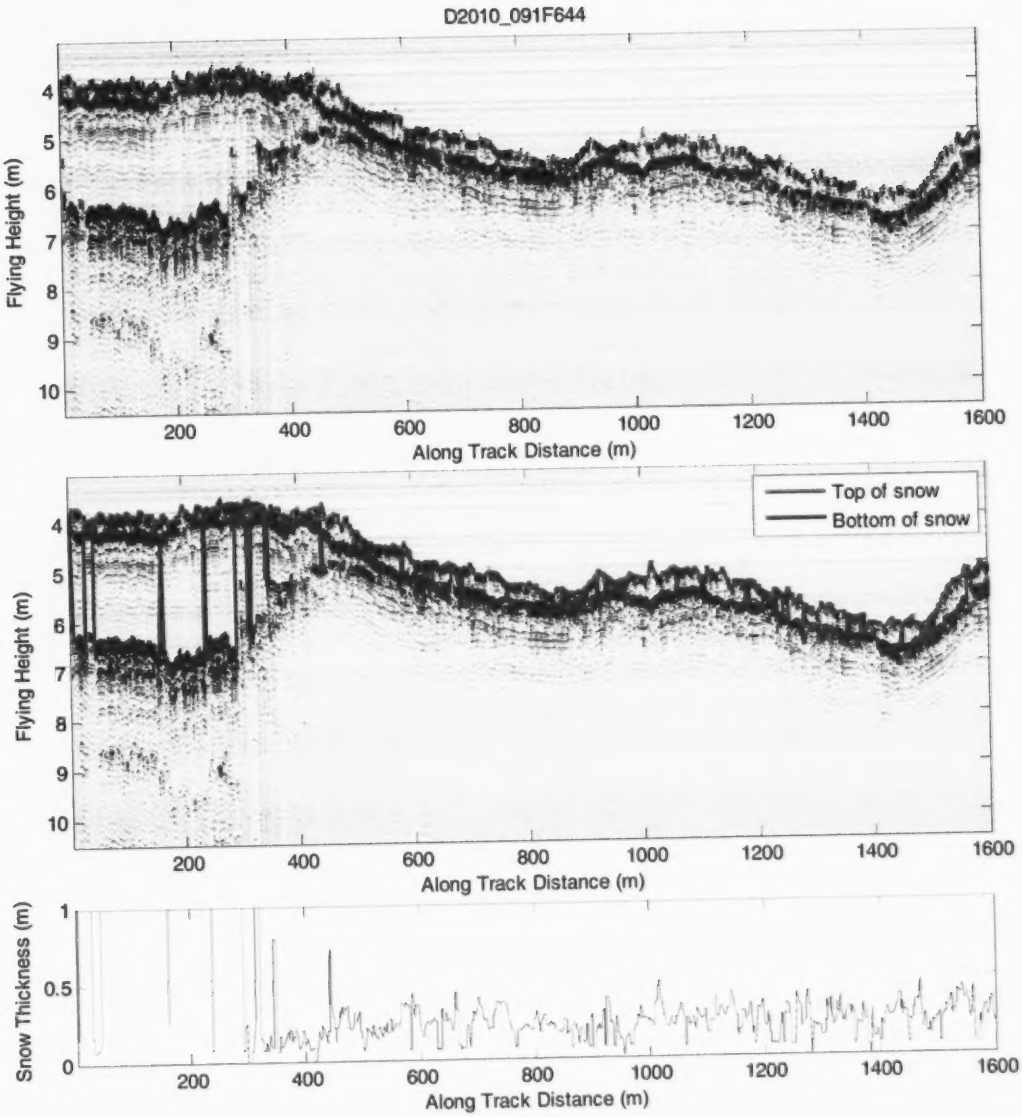

Plot of the first quarter of the GPR profile 644

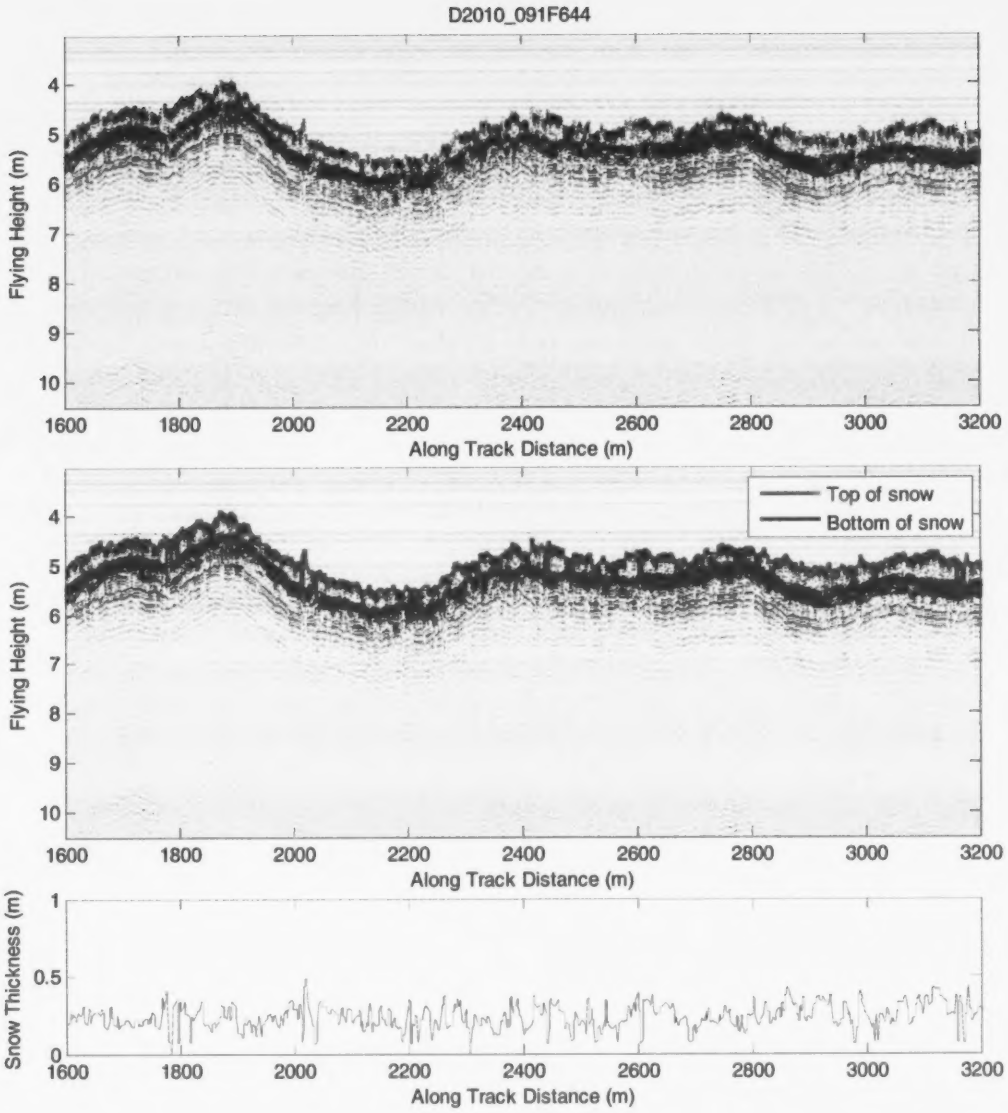

Plot of the second quarter of GPR profile 644

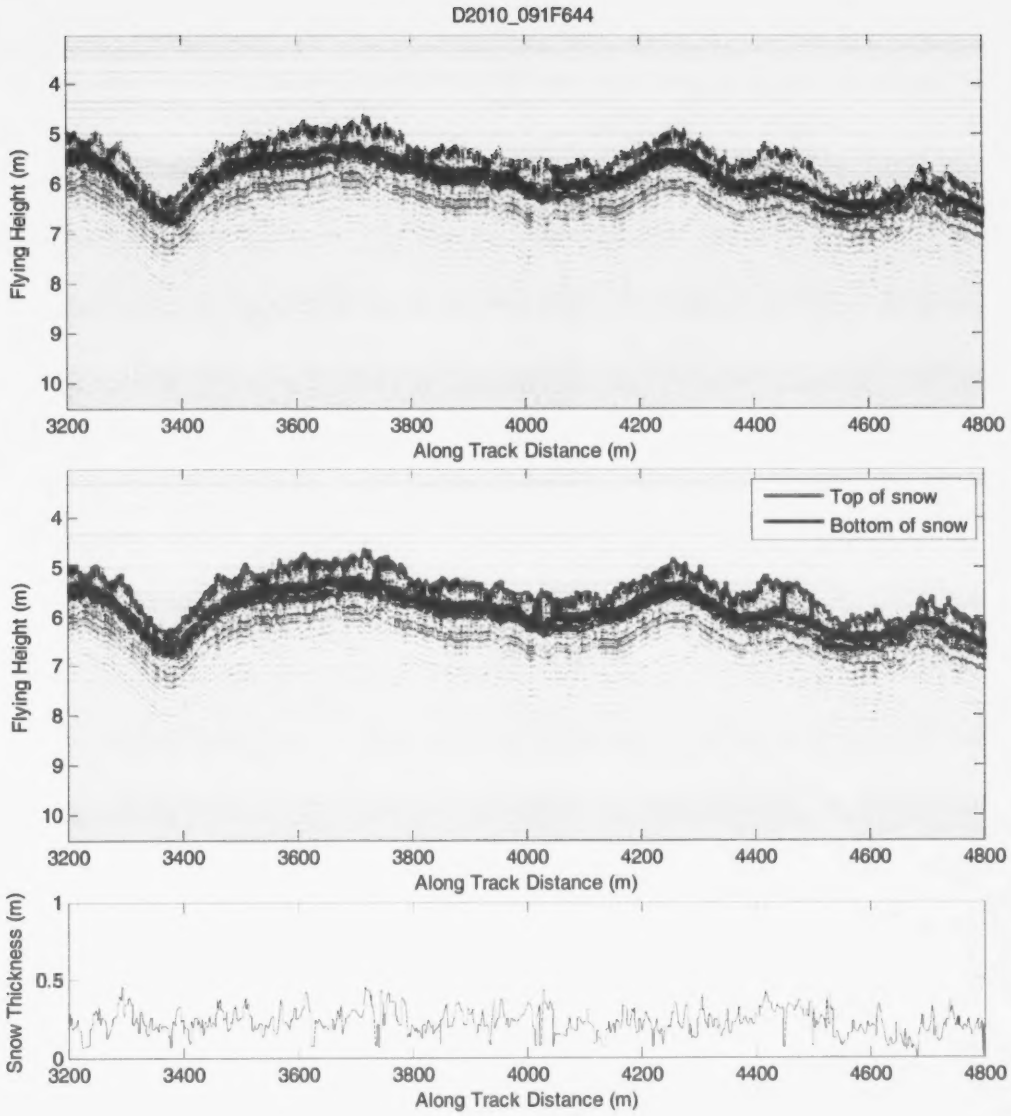

Plot of the third quarter of GPR profile 644

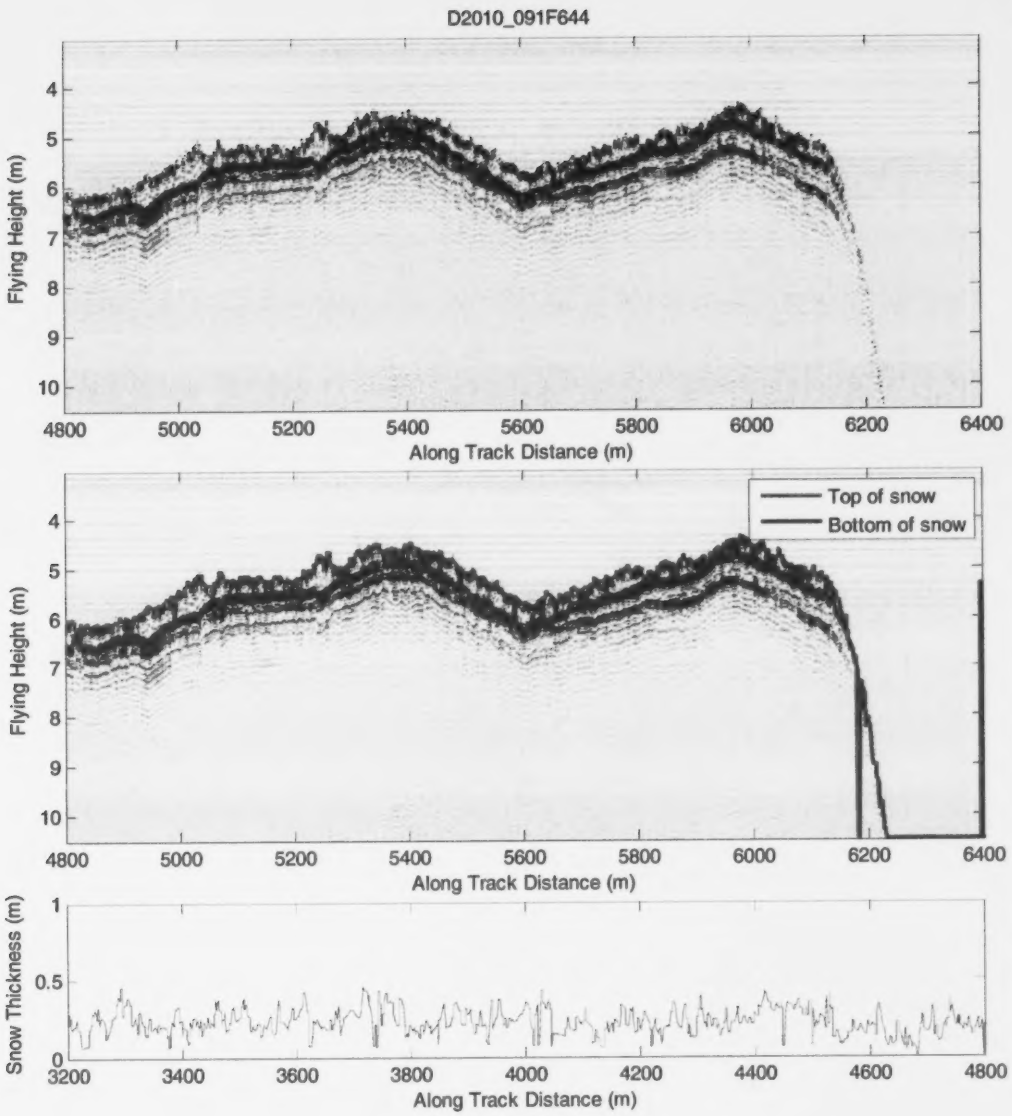

Plot of the last quarter of GPR profile 644

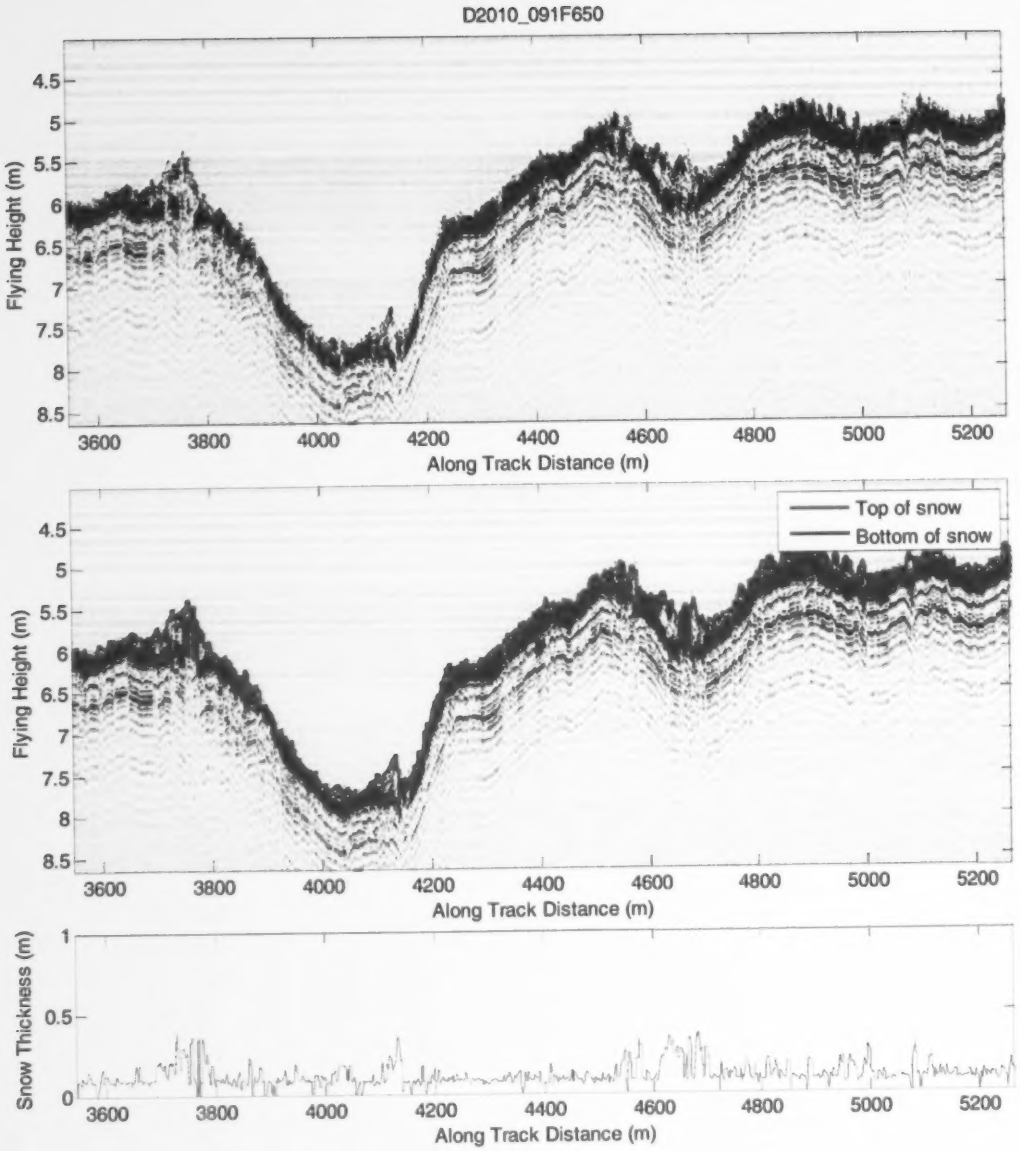

Plot of the part of GPR profile 650

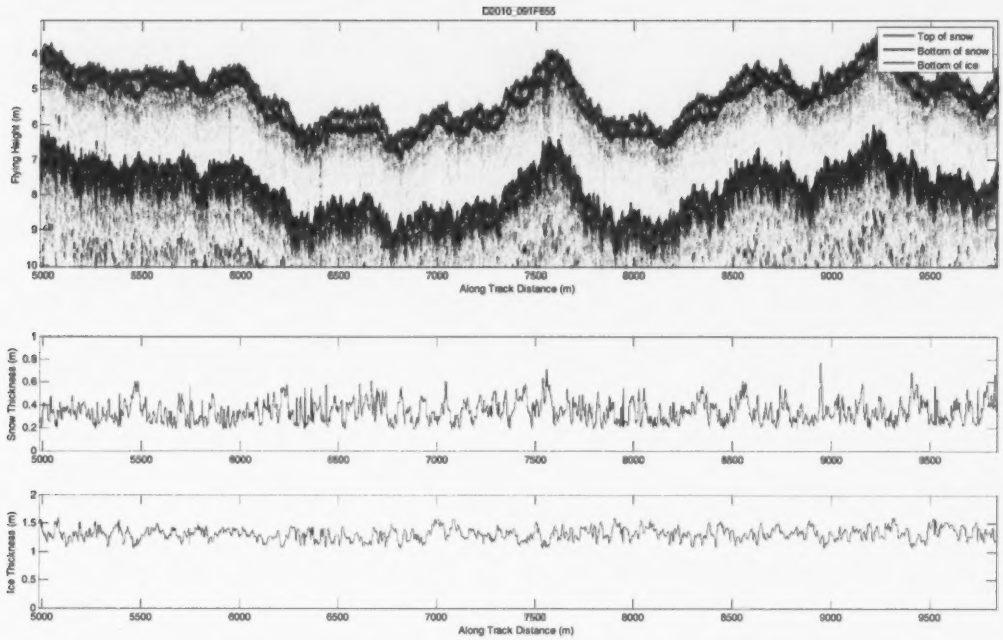

Plot of the total GPR profile 650 (~ 5km) showing snow depths and freshwater ice thickness line plots (Figure also in main text as Fig. 17)